Published in "Journal of Cell Science 128(13): 2278–2292, 2015"
which should be cited to refer to this work.

The I-BAR protein Ivy1 is an effector of the Rab7 GTPase Ypt7 involved in vacuole membrane homeostasis

Johannes Numrich[1], Marie-Pierre Péli-Gulli[2], Henning Arlt[1], Alessandro Sardu[2], Janice Griffith[3], Tim Levine[4], Siegfried Engelbrecht-Vandré[1], Fulvio Reggiori[3], Claudio De Virgilio[2] and Christian Ungermann[1,*]

ABSTRACT

Membrane fusion at the vacuole depends on a conserved machinery that includes SNAREs, the Rab7 homolog Ypt7 and its effector HOPS. Here, we demonstrate that Ypt7 has an unexpected additional function by controlling membrane homeostasis and nutrient-dependent signaling on the vacuole surface. We show that Ivy1, the yeast homolog of mammalian *missing-in-metastasis* (MIM), is a vacuolar effector of Ypt7-GTP and interacts with the EGO/ragulator complex, an activator of the target of rapamycin kinase complex 1 (TORC1) on vacuoles. Loss of Ivy1 does not affect EGO vacuolar localization and function. In combination with the deletion of individual subunits of the V-ATPase, however, we observed reduced TORC1 activity and massive enlargement of the vacuole surface. Consistent with this, Ivy1 localizes to invaginations at the vacuole surface and on liposomes in a phosphoinositide- and Ypt7-GTP-controlled manner, which suggests a role in microautophagy. Our data, thus, reveal that Ivy1 is a novel regulator of vacuole membrane homeostasis with connections to TORC1 signaling.

KEY WORDS: Ivy1, Ypt7, Vps33, TORC1, EGO complex, Vacuole biogenesis

INTRODUCTION

The yeast vacuole is equivalent to the mammalian lysosome and is required to degrade macromolecules, such as proteins and lipids, in its hydrolytic environment and make the resulting metabolites available for the cell.

Several trafficking pathways, such as the endocytic and the AP-3 pathway, as well as autophagy, direct cargo to the vacuole and require the Rab7 GTPase Ypt7 for the final fusion event (Haas et al., 1995; Wichmann et al., 1992). Ypt7 is – like all Rab proteins – a switch-like protein that is converted to its active GTP-bound form by the dimeric Mon1–Ccz1 complex, an endosomal guanine nucleotide exchange factor (GEF) (Gerondopoulos et al., 2012; Nordmann et al., 2010; Cui et al., 2014; Singh et al., 2014). The active form of Ypt7 can bind to several effectors that have been implicated in membrane trafficking. On endosomes, Ypt7-GTP interacts with the retromer complex and, thus, supports recycling of transport receptors back to the Golgi complex (Balderhaar et al., 2010; Liu et al., 2012). For fusion of endosomes with vacuoles, Ypt7 binds to the hexameric HOPS tethering complex through its subunits Vps41 and Vps39 (Bröcker et al., 2012; Seals et al., 2000; Wurmser et al., 2000), which is followed by SNARE-mediated fusion (Stroupe et al., 2009).

The role of Rab GTPases in events not directly connected to membrane trafficking is an emerging theme. For instance, Ypt7 acts in the formation of a contact zone between vacuoles and mitochondria (Elbaz-Alon et al., 2014; Hönscher et al., 2014). Metazoan Rab7 has also been linked to cellular signaling, and interacts with the PI-3-kinase Vps34 that is similar to Rab5 (Shin et al., 2005; Stein et al., 2003). Likewise, Rab5 and its yeast homolog Vps21 have functions beyond membrane fusion (Durán and Hall, 2012; Numrich and Ungermann, 2014). Rab5 binds the transcription factor APPL and, thus, regulates cell proliferation (Miaczynska et al., 2004), whereas Vps21 affects cellular Ca^{2+} signaling (Nickerson et al., 2012).

Over the last years, it has become clear that the lysosome is a central hub for cellular signaling (Bar-Peled and Sabatini, 2012; Jewell et al., 2013; Wullschleger et al., 2006). The surface of yeast vacuoles harbors the EGO complex, which contains the Ego1 membrane protein Ego3, and the two Rag GTPases Gtr1 and Gtr2 (Binda et al., 2009; Bonfils et al., 2012; Dubouloz et al., 2005; Zhang et al., 2012). A similar heptameric complex, called LAMTOR, has been identified in metazoan cells (Bar-Peled et al., 2012; Sancak et al., 2010). The EGO–LAMTOR complex binds to the target of rapamycin complex 1 (TORC1), which is also found on yeast vacuoles and mammalian lysosomes (Berchtold and Walther, 2009; Sturgill et al., 2008).

Loss of TORC1 activity results in induction of autophagy that can be divided into macro- and microautophagy (Chen and Klionsky, 2011; Mizushima et al., 2011). Microautophagy is known to sequester specific cargos or cytosolic portions into inward protrusions at the vacuolar or lysosomal surface, and has been described as a mechanism to selectively degrade mitochondria, peroxisomes, lipid droplets, parts of the ER, and parts of the nucleus (Bernales et al., 2006; Böckler and Westermann, 2014; Roberts et al., 2003; Schuck et al., 2014; van Zutphen et al., 2014; Wang et al., 2014). All these processes are largely dependent on the core machinery of autophagy consisting of 18 autophagy-related genes (ATG) genes, but the mechanism how invaginations are formed is poorly understood.

Interestingly, TORC1 activity has been linked to the subunits of the HOPS complex and Rab7 (Flinn et al., 2010; Zurita-Martinez et al., 2007), leading to the question about how trafficking and amino-acid sensing are coordinated. In this study, we identify Ivy1, an inverse (I)-BAR protein, as an effector of Ypt7 on vacuoles, that we link to membrane dynamics and TORC1 activity. Our results show that Ypt7, in complex with Ivy1, could coordinate cellular signaling and/or the regulation of metabolism, and homeostasis of the vacuole membrane.

[1]University of Osnabrück, Department of Biology/Chemistry, Biochemistry section, Barbarastrasse 13, 49076 Osnabrück, Germany. [2]University of Fribourg, Department of Biology, Division of Biochemistry, Chemin du Musée 10, Fribourg CH-1700, Switzerland. [3]University Medical Centre Utrecht, Center for Molecular Medicine, Department of Cell Biology, Heidelberglaan 100, Utrecht 3584 CX, The Netherlands. [4]UCL Institute of Ophthalmology, Department of Cell Biology, 11-43 Bath St., London EC1V 9EL, UK.

*Author for correspondence (cu@uos.de)

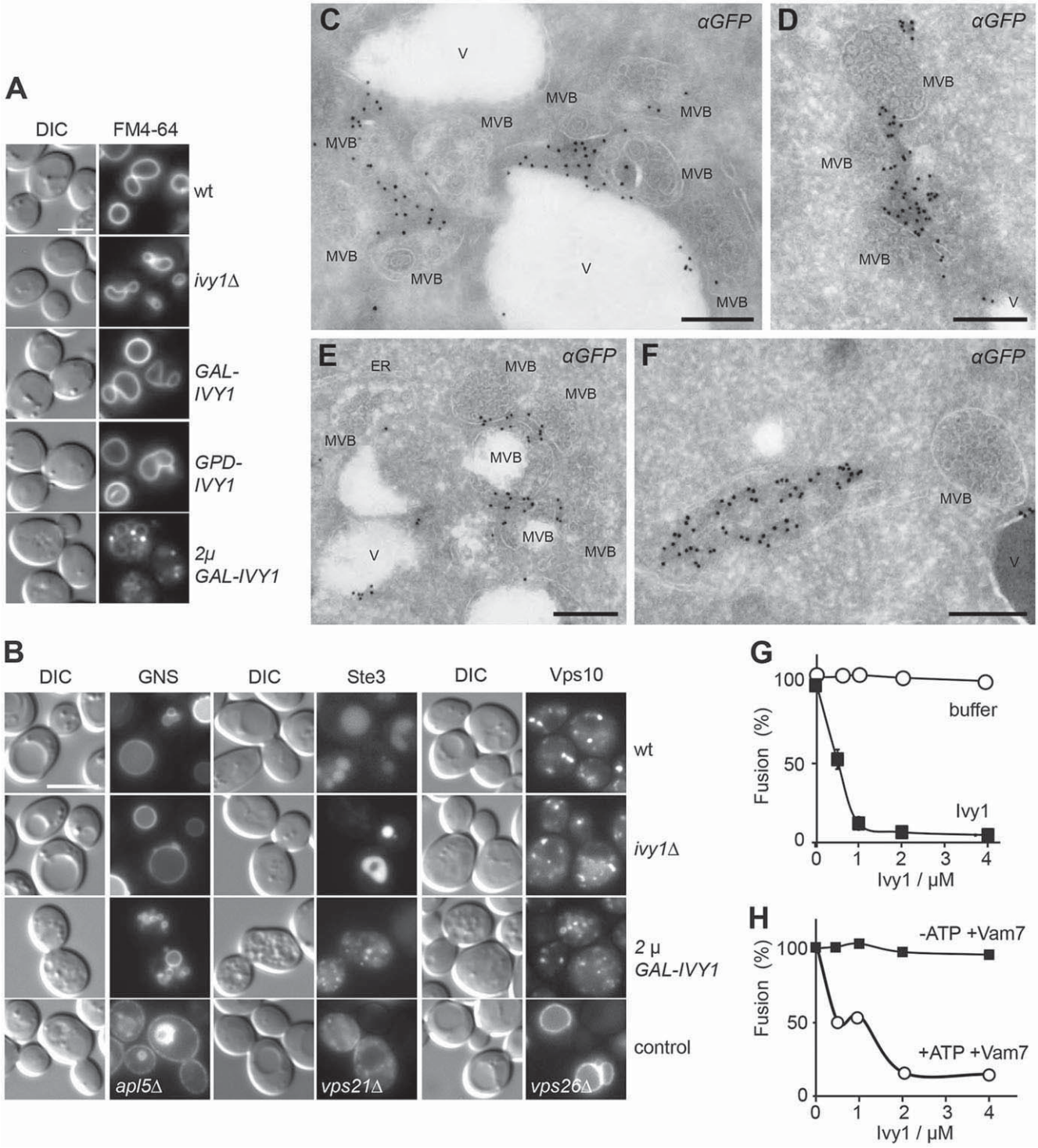

Fig. 1. Ivy1 overexpression affects vacuole morphology, fusion, and sorting. (A) Strong overexpression of Ivy1 results in vacuole fragmentation. WT, *ivy1*Δ or cells expressing *IVY1* from the indicated promoter under the control of the endogenous locus, or from a 2 μ plasmid, were grown in YPD or YPG (for galactose induction). Vacuoles were stained with FM4-64 and examined by fluorescence microscopy. Scale bar: 5 μm. (B) Effect of Ivy1 overexpression on protein sorting. Cells were similar as in A. To monitor AP-3 pathway trafficking, GFP-tagged Snc1 with a C-terminal transmembrane domain of Nyv1 (GNS) was expressed; a deletion of the AP-3 protein Apl5 was used as control. For endocytic trafficking, GFP-tagged Ste3 was monitored in comparison to *vps21*Δ cells, which have a defect in endocytic sorting. To observe endocytic recycling, GFP-tagged Vps10 was expressed in the indicated strains and compared with *vps26*Δ cells as a control. Size bar: 5 μm. (C–F) *IVY1* overexpression results in the accumulation of multivesicular bodies and cytosolic Ivy1 deposits. Cells expressing Ivy1-GFP from a *GPD1* promoter were analyzed by immunoelectron microscopy (see Materials and Methods). Ivy1 was detected by using anti-GFP antibodies and protein A-conjugated gold. MVB, multivesicular bodies; V, vacuole; ER, endoplasmic reticulum. Scale bars: 200 nm. (G) Recombinant Ivy1 inhibits *in vitro* vacuole fusion. His-tagged Ivy1 or buffer was added to the vacuole fusion reaction carrying vacuole from the two tester strains (BJ3505, *pep4*Δ and DKY6281, *pho8*Δ) at the indicated concentrations, and reactions were incubated for 90 min at 26°C before being analyzed. Vacuole fusion assay was performed as described in Materials and Methods. (H) Ivy1 behaves like an Ypt7-specific inhibitor. Vacuole fusion was carried out in the presence of 1 μM Vam7 with and without an ATP-regenerating system, and Ivy1 was added at the indicated concentrations. Reactions were processed as in G.

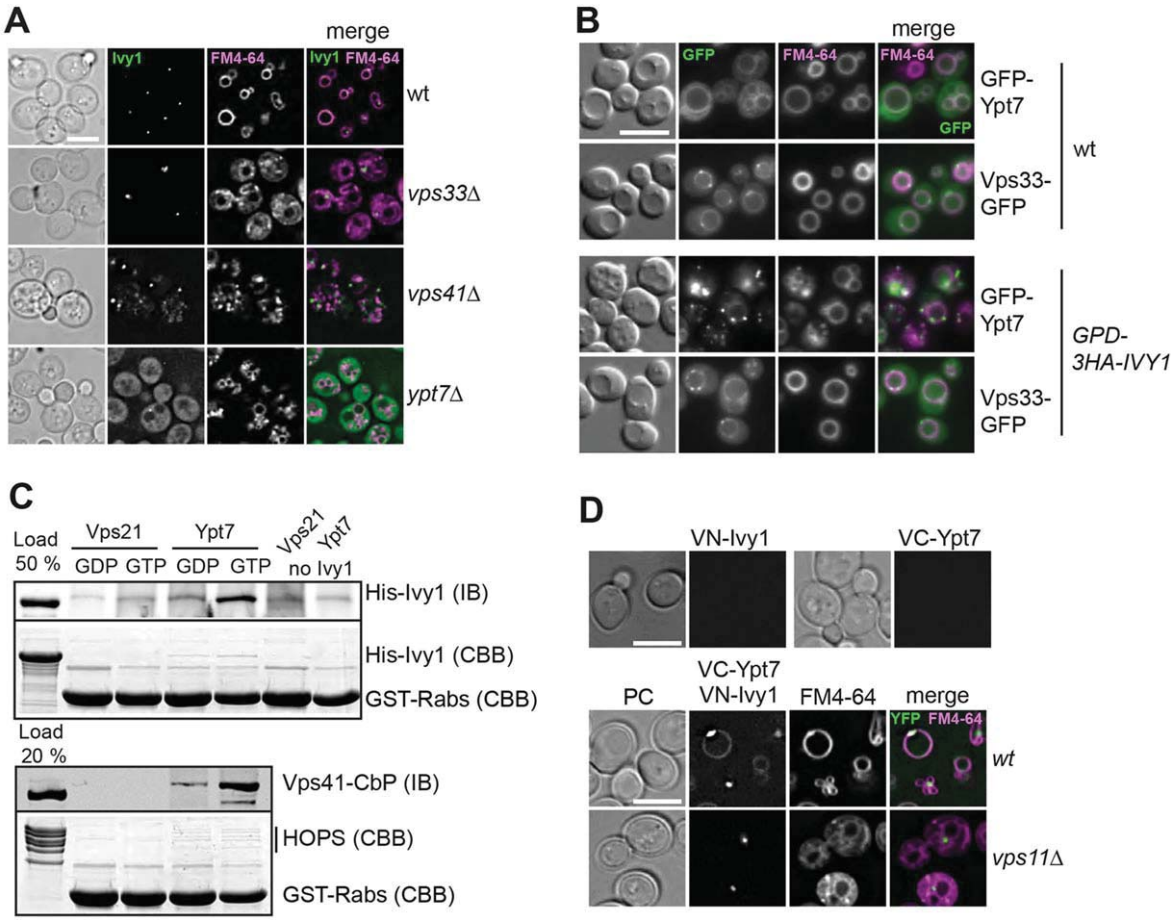

Fig. 2. Ivy1 is an effector of Ypt7. (A) Localization of Ivy1-GFP is dependent on Ypt7. Wild-type (wt) and the indicated deletion strains expressing Ivy1-GFP were grown to logarithmic growth phase, and stained with FM4-64 before being examined by fluorescence microscopy. Scale bar: 5 µm. (B) Ivy1 expression affects localization of Ypt7 but not Vps33. Cells expressing Ivy1 from the endogenous promoter or from the strong *GPD1* promoter, as well as GFP-tagged Vps33 and Ypt7 were analyzed by fluorescence microscopy. Note that GFP-Ypt7 refers to N-terminal tagging, whereas Vps33-GFP to C-terminal tagging. Scale bar: 5 µm. (C) Ivy1 interacts preferentially with Ypt7-GTP. Recombinant His-Ivy1 was applied to GST-tagged Rab GTPases that were preloaded with GDP or GTP and immobilized on GSH beads (top). Bound proteins were eluted, TCA precipitated and analyzed by western blotting (IB). Beads were boiled to elute Rab proteins and the remainder of bound protein, and proteins were visualized on SDS-PAGE gels stained with Coomassie Brilliant Blue (CBB). TAP-purified HOPS complex was used as control (bottom). For details see Materials and Methods. (D) Ivy1 interacts with Ypt7 *in vivo*. The split YFP method was used to detect interaction of Ivy1 and Ypt7 *in vivo*. Wild-type (wt) and *vps11*Δ cells expressing VN-Ivy1 and VC-Ypt7 were grown to logarithmic growth phase and analyzed by microscopy. Top row shows wt cells expressing either VN-Ivy1 or VC-Ypt7. Scale bars: 5 µm. PC, phase contrast.

RESULTS

Ivy1 can affect endocytic protein sorting and vacuole morphology

In a previous study, we used an overexpression screen to search for proteins affecting vacuolar morphology (Arlt et al., 2011). Strong overexpression of *S. cerevisiae IVY1* from the 2-µm plasmid resulted in massive vacuole fragmentation (Fig. 1A), which is in agreement with previous findings (Lazar et al., 2002). High cellular levels of this protein also caused defects in protein sorting along the endocytic pathway (Fig. 1B) (Arlt et al., 2011). Although vacuole delivery of cargo of the AP-3 pathway, the artificial fusion between GFP-tagged Snc1 and the transmembrane domain of the vacuolar v-SNARE Nyv1 (GNS), and Vps10 recycling from endosomes were not affected in cells overexpressing *IVY1*, the endocytosis of the Ste3 receptor was as defective as in *vps21*Δ cells, which lack the Rab5-like GTPase of endosomes (Fig. 1B). By using immuno-electron microscopy (IEM), ultrastructural analysis of the strain overexpressing *IVY1* revealed strong accumulation of multivesicular bodies proximal to the vacuole (Fig. 1C,D), and localized Ivy1 both on the vacuolar surface and in cytosolic filamentous protein aggregates between the MVBs (Fig. 1D–F). These data suggested that Ivy1, as an interactor of Ypt7 and/or the HOPS subunit Vps33 (Lazar et al., 2002), can control fusion on vacuoles and multivesicular bodies. To test this potential role of Ivy1 in controlling fusion, we purified recombinant Ivy1 and added it to the established vacuole fusion assay (Haas et al., 1994). This assay requires both Ypt7 and HOPS, and measures the luminal mixing of isolated vacuoles (see Materials and Methods). Addition of Ivy1 inhibited homotypic vacuole fusion efficiently (Fig. 1G,H). To find out whether Ivy1 acts on Ypt7, we performed the same titration experiment with Ivy1 in the absence of ATP but the presence of the SNARE Vam7 (Thorngren et al., 2004). Under these conditions, Ypt7 is tightly bound to HOPS (Brett and Merz, 2008; Cabrera et al., 2009; LaGrassa and Ungermann, 2005), and is relieved by phosphorylation of HOPS in the presence of ATP (LaGrassa and Ungermann, 2005). Ivy1 only inhibited fusion in the presence of ATP (Fig. 1H), suggesting that this protein directly interacts with Ypt7.

Ivy1 is an Ypt7-effector on vacuoles

To determine the relation of Ivy1 with Ypt7 and HOPS, we traced the GFP-tagged protein in wild-type and various deletion strains. In

wild-type cells, endogenous Ivy1 was present in distinct puncta on the vacuolar surface (Fig. 2A). This localization was not affected by deletion of its putative interaction partner, the HOPS subunit Vps33, or Vps41 – another HOPS subunit (Fig. 2A). In the absence of Ypt7, however, Ivy1 was almost entirely cytosolic, indicating that Ivy1 requires Ypt7 to localize to vacuoles (Fig. 2A). In agreement, overexpression of *IVY1* in cells that express GFP-tagged Ypt7 resulted in a strong relocalization of Ypt7 to dot-like structures that colocalized with the lipophilic dye FM4-64 (Fig. 2B). This suggests that the excess amount of Ivy1 traps Ypt7 at endosomes, which is in agreement with the observed accumulation of MVBs following ultrastructural analyses (Fig. 1C,D). In contrast, the subcellular distribution of Vps33 remained unaffected by overexpression of Ivy1 (Fig. 2B), indicating that the reported Vps33 interaction with Ivy1 (Lazar et al., 2002) is not important for intracellular function of Ivy1.

To test for direct interaction between Ivy1 and Ypt7, we incubated recombinant Ivy1 with purified GST-tagged Ypt7 or Vps21 that had been preloaded with GDP or GTPγS. Ivy1 was efficiently and specifically isolated together with Ypt7-GTP (Fig. 2C). The interaction is comparable to the interaction between Ypt7 and HOPS, which was analyzed in parallel to confirm that Ypt7 was loaded with GTP (Fig. 2C, bottom panel). To further verify the close proximity between Ivy1 and Ypt7, we used bimolecular fluorescence complementation, also known and hereafter referred to as split-YFP approach), where each protein is tagged either with the N-terminal (VN) or C-terminal (VC) segment of the Venus variant of GFP (Sung and Huh, 2007). The YFP-signal was, indeed, observed on vacuoles of wild-type cells and strongly diminished in those of *vps11*Δ cells, which have defective vacuoles (Fig. 2D). We, thus, conclude that Ivy1 is a so-far-unknown vacuolar effector of Ypt7.

Ivy1 interacts with the EGO–LAMTOR complex on vacuoles

If the Ypt7-dependent localization of Ivy1 were required to control fusion at the vacuole, one would expect colocalization with selected marker proteins of organelles involved in these events. Apart from the colocalization with Ypt7, we did not detect overlapping localization with the mCherry-tagged ESCRT-III subunit Snf7, the vacuolar Vac8 protein found at nuclear vacuolar junction (NVJs) (Pan et al., 2000) or with mitochondria, which form a recently identified contact site with vacuoles termed vCLAMP (Elbaz-Alon et al., 2014; Hönscher et al., 2014) (Fig. 3A). Similarly, the Atg8-positive pre-autophagosomal structure (PAS) (seen in Fig. 3A, bottom images, in the cell to the left) did not overlap with Ivy1 on vacuoles (shown in enlargement).

As our data did not agree with a role for Ivy1 in endosomal fusion, we searched for other proteins that colocalized on the vacuole. We previously have characterized the palmitoylated Ego1/Meh1 protein on vacuoles (Hou et al., 2005), which is part of the EGO complex comprising Ego1, Ego3, and the two Rag GTPases Gtr1 and Gtr2 (Dubouloz et al., 2005; Levine et al., 2013; Zhang et al., 2012). The yeast EGO complex and mammalian LAMTOR both activate TORC1 in the presence of amino acids (Bar-Peled et al., 2012; Binda et al., 2009; Bonfils et al., 2012; Dubouloz et al., 2005). Interestingly, the HOPS subunit Vps39, which requires Ypt7 for its vacuolar localization (Bröcker et al., 2012), colocalizes with the EGO complex and has been implicated in EGO function (Binda et al., 2009). We, therefore, localized Ivy1 relative to EGO components, and observed both Ivy1 and EGO components in the same domains on vacuoles (Fig. 3B) that also localized with Ypt7 and Vps39 (Fig. 3C) (Binda et al., 2009).

To test for close proximity to the EGO complex, we utilized again the split-YFP approach. Within this analysis, we observed a clear and specific signal when Ivy1-VC was expressed with Gtr2-VN or Ego3-VN, and a weak signal when it was expressed with Iml1-VN (Fig. 3D), the identified GTPase activating protein (GAP) of Gtr1 (Bar-Peled et al., 2013; Panchaud et al., 2013). VN-Gtr2 did not yield any signal, suggesting that the position of the tag could bias the read-out of this assay. Together, these data suggest that Ivy1, indeed, localized to the vicinity of the EGO complex. To further substantiate these findings, we used the membrane-based split-ubiquitin two-hybrid system (Nikko and Andre, 2007) and, again, observed interactions of Ivy1 with components of the EGO complex, such as Gtr1 (Fig. 3E). Gtr2 was not detected here, presumably because of the same tag-related problem as in the split-YFP assay. Additionally, Ivy1 strongly interacted with itself (Fig. 3E), indicating that the protein forms dimers or oligomers as suggested by the IEM analysis (Fig. 1C,D). We conclude that Ivy1 is, indeed, proximal to the EGO complex on the vacuole, which might provide a functional link.

A link between Ivy1 and TORC1 signaling on vacuoles

We next wondered whether the proximity of Ivy1 to the EGO complex has functional consequences on TORC1 signaling. Deletion of *IVY1* alone did not affect the localization of EGO to dot-like structures on vacuoles as revealed by Ego3-GFP distribution (Fig. 3F), indicating that Ivy1 is not a structural component that is responsible for the localization of the EGO complex. Vice versa, deletion of EGO subunits such as Ego3 did not change the localization of Ivy1 (Fig. 3G). Thus, Ivy1 and EGO are not necessary for localization of each other but may have a functional relationship. We, thus, used growth assays in the presence of the well-established TORC1 inhibitor rapamycin. Growth on rapamycin-containing plates identifies mutants that cause defects in TORC1 activation. Consequently, deletion of *EGO1* or *EGO3* results in a growth defect on rapamycin. However, *ivy1*Δ cells did not show any growth impairment on rapamycin (Fig. 4A). We speculated that Ivy1 might affect TORC1 activity more indirectly or even act as a negative regulator. Under these conditions, a growth defect on rapamycin-containing plates would not be expected for *ivy1*Δ cells.

We, therefore, searched for conditions under which Ivy1 is important or essential for growth and, thus, crossed *ivy1*Δ cells against the entire deletion library of viable yeast-knockout strains and analyzed the growth phenotype of the respective double mutants (Tong et al., 2001). Among the respective double mutants that were most seriously compromised for growth were those, in which *ivy1*Δ was combined with mutations within specific subunits of the V-ATPase (Fig. 4B). This was an interesting observation because the V-ATPase has been identified as a possible sensor of amino acid availability within the vacuole (Zoncu et al., 2011). In addition, the V-ATPase is involved in acidification of the vacuole, which can be bypassed by growing cells in low pH medium – as shown for the *vma2* mutant – but results in sensitivity to high pH (Fig. 4C). Since *ivy1*Δ cells did not show sensitivity, we excluded a function regarding the regulation of vacuolar pH (Fig. 4C).

We next analyzed the effects of loss of Ivy1 in combination with loss of individual V-ATPase subunits in our assays, and focused primarily on the *ivy1*Δ *vma16*Δ mutant. Because of the connection to TORC1, we tested this double mutant for its sensitivity to rapamycin. Under the conditions applied, the *ivy1*Δ *vma16*Δ double knockout was hypersensitive to rapamycin, as known for *ego1*Δ cells (Fig. 4D). We then tested whether the TORC1 activity in these strains was reduced as expected, and thus analyzed the phosphorylation status of the TORC1 target Sch9 to this end (Urban et al., 2007). Although each single deletion incurred only a minor defect in TORC1 activity, the *ivy1*Δ *vma16*Δ double mutant was strongly impaired (Fig. 4E,F). This defect is not due to reduced proteolytic activity of the mutant vacuoles

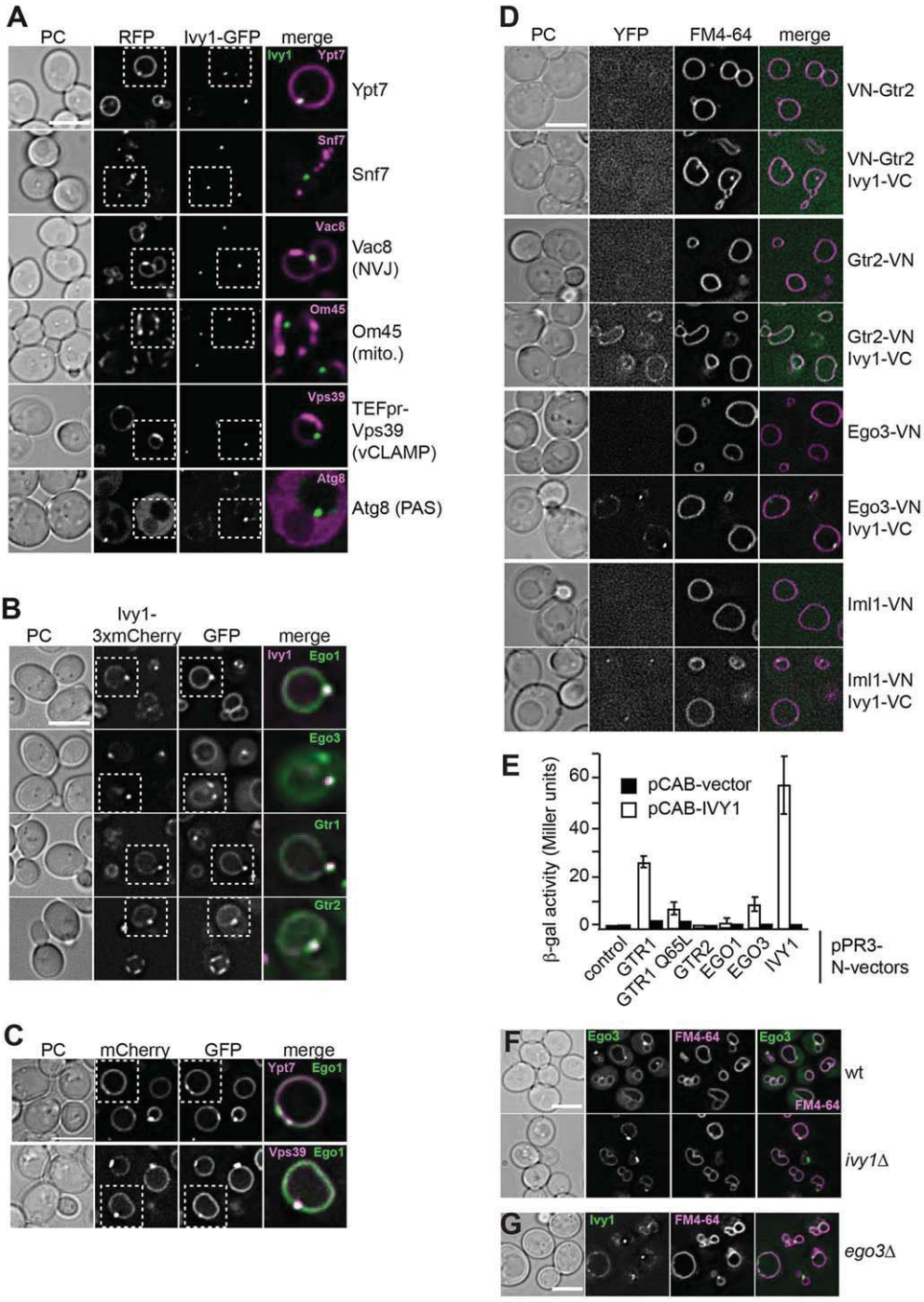

Fig. 3. Ivy1 colocalizes and interacts with the EGO complex. (A) Distribution of Ivy1-GFP on vacuoles relative to other vacuolar markers, membrane contact sites and other organelles. Cells expressing Ivy1-GFP and the indicated RFP-tagged marker proteins [Ypt7=vacuole, Snf7=endosomes, Vac8=nuclear vacuolar junctions (NVJ), OM45=mitochondria, Vps39=vCLAMP, Atg8=preautophagosomal membrane (PAS)] were grown to logarithmic growth phase and analyzed by microscopy. Scale bar: 5 µm. Regarding its localization in respect to Atg8, Ivy1 was never found in the same focal plane as Atg8, so we concluded that they do not colocalize. Vps39 was overexpressed to facilitate visualization of vCLAMPs (Elbaz-Alon et al., 2014; Hönscher et al., 2014). (B) Ivy1 colocalizes with subunits of the EGO complex. Cells expressing Ivy1-3xmCherry and GFP-tagged subunits of the EGO complex (Ego1, Ego3, Gtr1, Gtr2) were grown to logarithmic growth phase and analyzed by microscopy. Scale bar: 5 µm. (C) The EGO complex colocalizes with Ypt7 and Vps39. Cells expressing GFP-tagged subunits of the EGO complex and either mCherry-Ypt7 or mCherry-Vps39 were grown to logarithmic growth and analyzed by microscopy. Scale bar: 5 µm. (D) Ivy1 interacts with subunits of the EGO complex and Iml1 in a split-YFP assay. Interactions were tested using cells expressing VN-tagged Gtr2, Ego3 or Iml1 without or with Ivy1-VC. Interactions were confirmed by microscopy. Note that VN-Gtr2 reflects N-terminal tagging, whereas Gtr2-VN C-terminal tagging. Scale bar: 5 µm. (E) Interaction of Ivy1 with subunits of the EGO complex. Interactions were tested by monitoring β-galactosidase activities (in Miller units) of cells expressing the N-terminal part of ubiquitin (Nub)-Ivy1 from the pCAB vector and the C-terminal part of ubiquitin (Cub)-tagged subunits of the EGO complex from the pPR3-N vector. Interactions of Ivy1 (bait) with EGOC components (prey) were assessed using the split-ubiquitin-based membrane two-hybrid system (Dualsystems Biotech AG). For each combination tested, β-galactosidase activity is expressed in Miller units as mean±s.d. from three independent transformants. As bait and prey control, empty pCABWT and pDL2-Alg5 vectors were used, respectively. (F) Localization of Ego3 in the absence of Ivy1. Ego3, tagged with GFP, was monitored relative to FM4-64 stained vacuoles. Scale bar: 5 µm. (G) Localization of Ivy1 in an EGO mutant background. Ivy1 was tagged with GFP in the *ego3*Δ strain that was stained with FM4-64, and localization was monitored as in A. Scale bar: 5 µm.

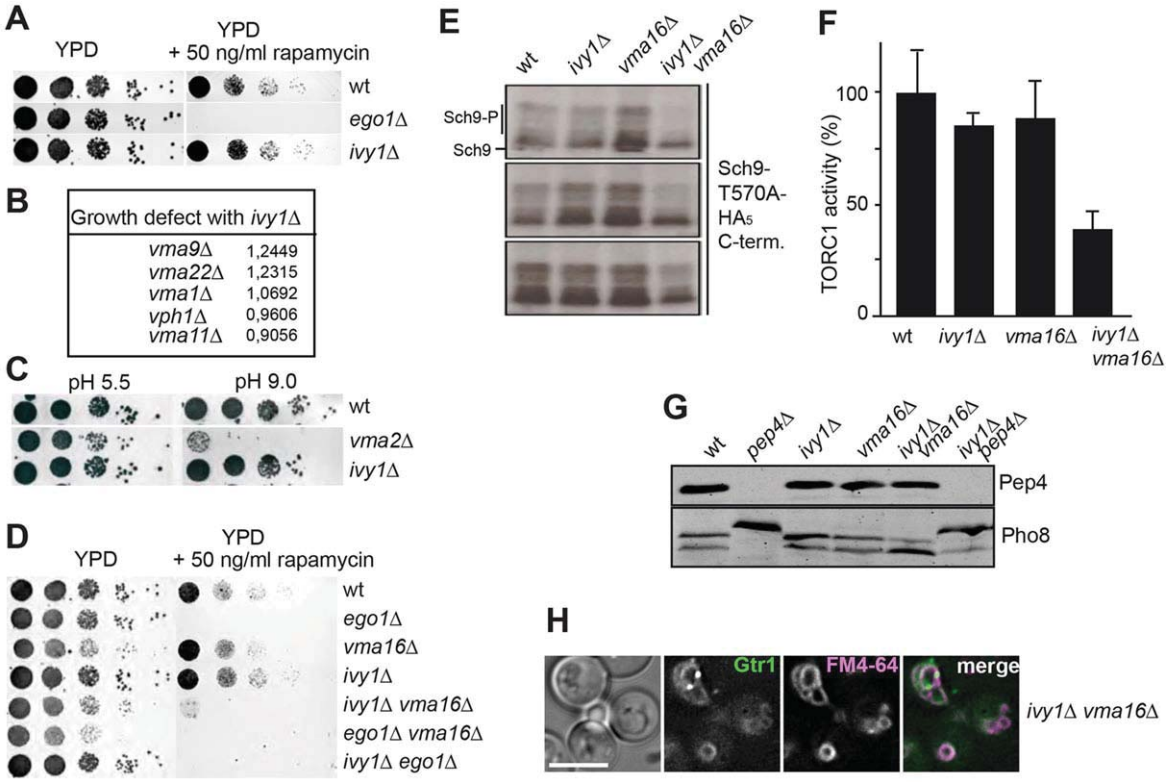

Fig. 4. A connection of Ivy1 to TORC1 activity. (A) Sensitivity to rapamycin. Serial dilutions of indicated strains were spotted on YPD or YPD +50 ng/ml rapamycin plates and photographed after 2 or 4 days (YPD or YPD +rapamycin, respectively) at 30°C. (B) Result from a synthetic genetic array screen with *ivy1*Δ. The *ivy1*Δ strain was crossed against the yeast-deletion library. Double mutants were further analyzed for growth defects. The table depicts V-ATPase mutants, which were among the strongest negative interactors when combined with *ivy1*Δ. (C) Unlike V-ATPase mutants, *ivy1*Δ is not pH sensitive. Serial tenfold dilutions of indicated strains were spotted on YPD with pH 5.5 or pH 9.0 and photographed after 2 days at 30°C. (D) The *ivy1*Δ *vma16*Δ double mutant exhibits increased sensitivity to rapamycin. Serial tenfold dilutions of indicated strains were spotted on YPD or YPD+50 ng/ml rapamycin plates and photographed after 2 or 4 days at 30°C. (E-F). The *ivy1*Δ *vma16*Δ double mutant shows reduced TORC1 activity. TORC1 activity was measured by analyzing the ratio of the phosphorylated to non-phosphorylated version of the Sch9 substrate in three independent assays as described in Materials and Methods (E). Quantification (wt TORC1 activity was set to 100%) is shown in F. (G) Vacuolar proteolytic activity is maintained in the absence of Ivy1 and the V-ATPase. Equal amounts of indicated strains were TCA precipitated and analyzed by SDS-PAGE and western blotting. The blot shows expression of Pep4 and Pep4-dependent processing of Pho8. (H) Localization of the EGO complex is not affected in *ivy1*Δ *vma16*Δ cells. Gtr1-GFP was monitored relative to FM4-64 in the respective cells. Scale bar: 5 µm.

because processing of the vacuolar alkaline phosphatase was still functional in *ivy1*Δ *vma16*Δ cells, but lost when the general peptidase Pep4 is absent (Fig. 4G). This suggests that the loss of TORC1 activity analyzed under these conditions is probably not owing to a problem in the acidification of the vacuole lumen. Furthermore, localization of the EGO complex is not influenced in the *ivy1*Δ *vma16*Δ mutant (Fig. 4H).

Ivy1 maintains vacuole membrane homeostasis

To unravel the reason for the growth defect on rapamycin and the reduced TORC1 activity, we analyzed the morphology of *ivy1*Δ *vma16*Δ vacuoles. Surprisingly, we noticed strong accumulation of membranous material in the vacuole lumen, which was stained by the lipophilic dye FM4-64 (Fig. 5A). Similar observations were made when a *vma6*Δ deletion with a defect in a V_0-ATPase subunit was combined with *ivy1*Δ, indicating that the general loss of V-ATPase activity causes in the same phenotype. To understand the origin of these membranous structures, we examined the double mutant at ultrastructural level by electron microscopy and observed numerous large vesicles whose content was indistinguishable from the cytoplasm within the vacuole lumen (Fig. 5B). We hypothesize that these structures are autophagosomes and, therefore, analyzed the efficiency of autophagy by monitoring the processing of GFP-Atg8 to free GFP – a standard method to assess the progression of this pathway (Klionsky et al., 2012) – when cells were starved by nitrogen (Fig. 5C). Whereas wild-type and *ivy1*Δ cells showed similar profiles of GFP-Atg8 processing, autophagy was already induced in *vma16*Δ cells during vegetative growth (as indicated by free GFP at the first time point) and increased over time. However, additional deletion of *IVY1* did not enhance this process. We, therefore, asked whether the vesicular structures in the vacuole of *ivy1*Δ *vma16*Δ cells are the results of the fusion of autophagosomes. When we monitored these cells by fluorescence microscopy, we noticed that, when stained with the vacuole-specific dye CMAC, the vacuole lumen but not the vesicular structures was positive for GFP-Atg8, a marker protein for autophagosomes (Fig. 5D). This suggests that these vesicles are connected to the vacuolar surface. To examine this in more detail, we recorded *Z*-stacks of vacuoles, and confirmed that the apparent vesicular structures are, indeed, continuous with the vacuole limiting membrane (Fig. 5E, supplementary material Movie S1). Thus, *ivy1*Δ *vma16*Δ vacuoles do not accumulate vesicles inside the lumen but have an enlarged and invaginated vacuolar surface.

As the deletion of *VMA16* already leads to increase of basal autophagy, we asked whether the same phenotype also occurs when we combine EGO mutants (which have lesser TORC1 activity) with the deletion of *ivy1*. Neither loss of EGO activity in an *ivy1*Δ mutant nor the increase of EGO activity (due to deletion of *IML1*) in a *ivy1*Δ *vma16*Δ double mutant affected the expanded membrane phenotype (Fig. 5F). This suggests that Ivy1 is more directly involved in

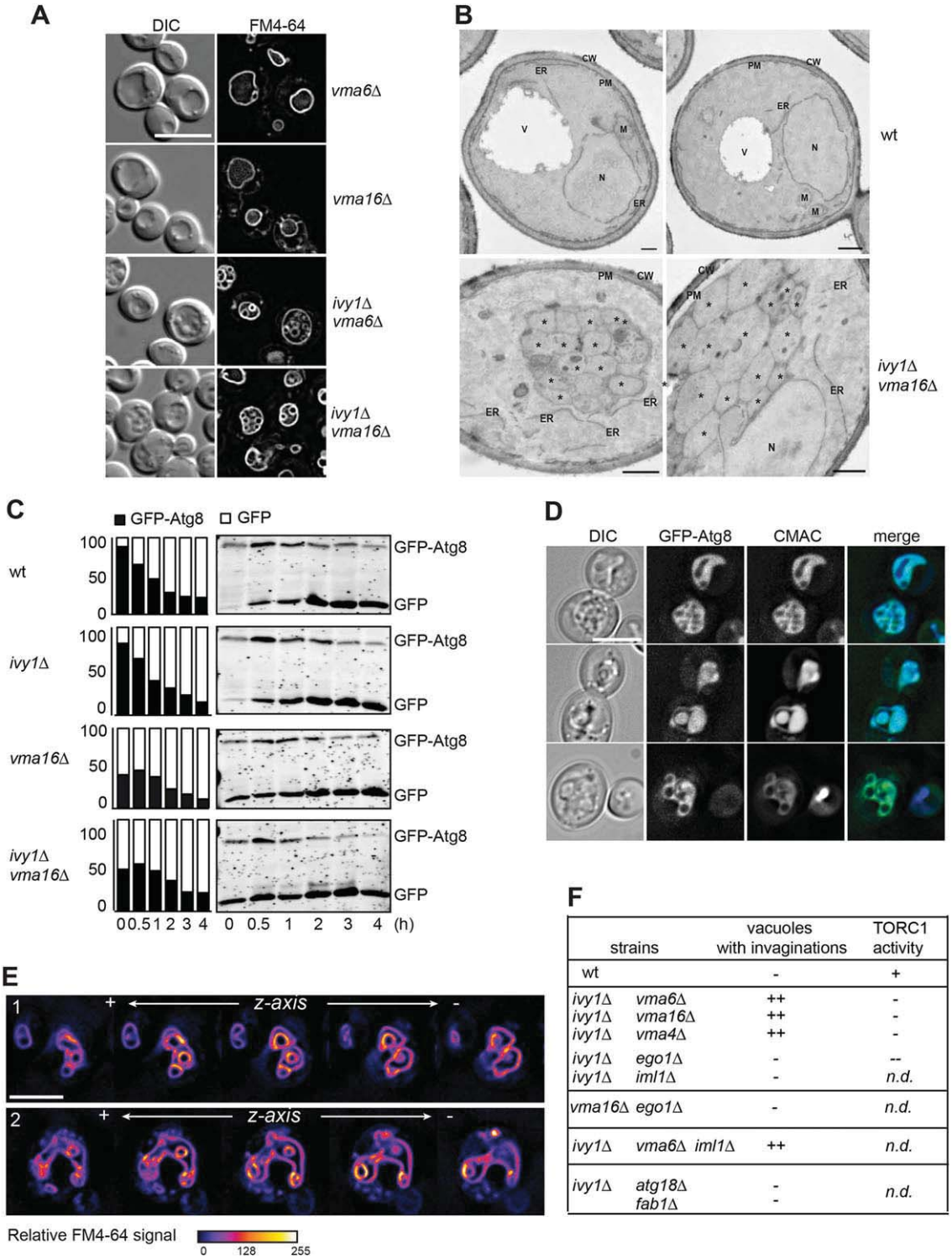

strains		vacuoles with invaginations	TORC1 activity
wt		-	+
ivy1Δ	*vma6Δ*	++	-
ivy1Δ	*vma16Δ*	++	-
ivy1Δ	*vma4Δ*	++	-
ivy1Δ	*ego1Δ*	-	--
ivy1Δ	*iml1Δ*	-	*n.d.*
vma16Δ	*ego1Δ*	-	*n.d.*
ivy1Δ	*vma6Δ iml1Δ*	++	*n.d.*
ivy1Δ	*atg18Δ*	-	*n.d.*
	fab1Δ	-	

Fig. 5. Ivy1 is required for vacuole membrane homeostasis. (A) Morphological analysis of the *ivy1Δ vma16Δ* double mutants. Vacuoles of indicated strains were stained for FM4-64 and analyzed by microscopy. Scale bar: 5 µm. (B) Ultrastructural analysis of *ivy1Δ vma16Δ* cells. Wt and *ivy1Δ vma16Δ* double mutant cells were analyzed by electron microscopy (see Materials and Methods). Scale bar: 200 nm top left panel; 500 nm other panels. V, vacuole; PM, plasma membrane; ER, endoplasmic reticulum; N, nucleus. (C) Analysis of autophagy. wt, *ivy1Δ*, *vma16Δ* and *ivy1Δ vma16Δ* cells were grown to logarithmic growth phase, then centrifuged and grown for the indicated time in nitrogen-depleted medium. Induction of autophagy was assessed by following processing of GFP-Atg8. Quantification of the ratio of GFP to GFP-Atg8 at each time point is displayed to the left, corresponding gels are shown to the right. (D) GFP-Atg8 localizes within vacuoles of *ivy1Δ vma16Δ* cells. *ivy1Δ vma16Δ* cells expressing GFP-Atg8 were grown to logarithmic growth phase and stained with CMAC. Figure shows different examples of vacuoles to display the vacuole variety. Scale bar: 5 µm. (E) Analysis of the vacuole morphology of *ivy1Δ vma16Δ* cells. *ivy1Δ vma16Δ* cells were grown to logarithmic growth phase, stained with FM4-64 and analyzed by fluorescence microscopy. Z-stacks of ten focal planes were recorded and five central layers are shown. Images were processed using ImageJ software. The color mode fire was used to highlight the relative differences in signal intensities within the focal planes. Scale bar: 2.5 µm. (F) Analysis of vacuole invaginations in mutants. The shown double mutants were analyzed for vacuole morphology as in A. The indicated strains were also analyzed for TOR activity as described in Fig. 4E-F. The *ivy1Δ vma6Δ* mutant was selected as the strongest example (++).

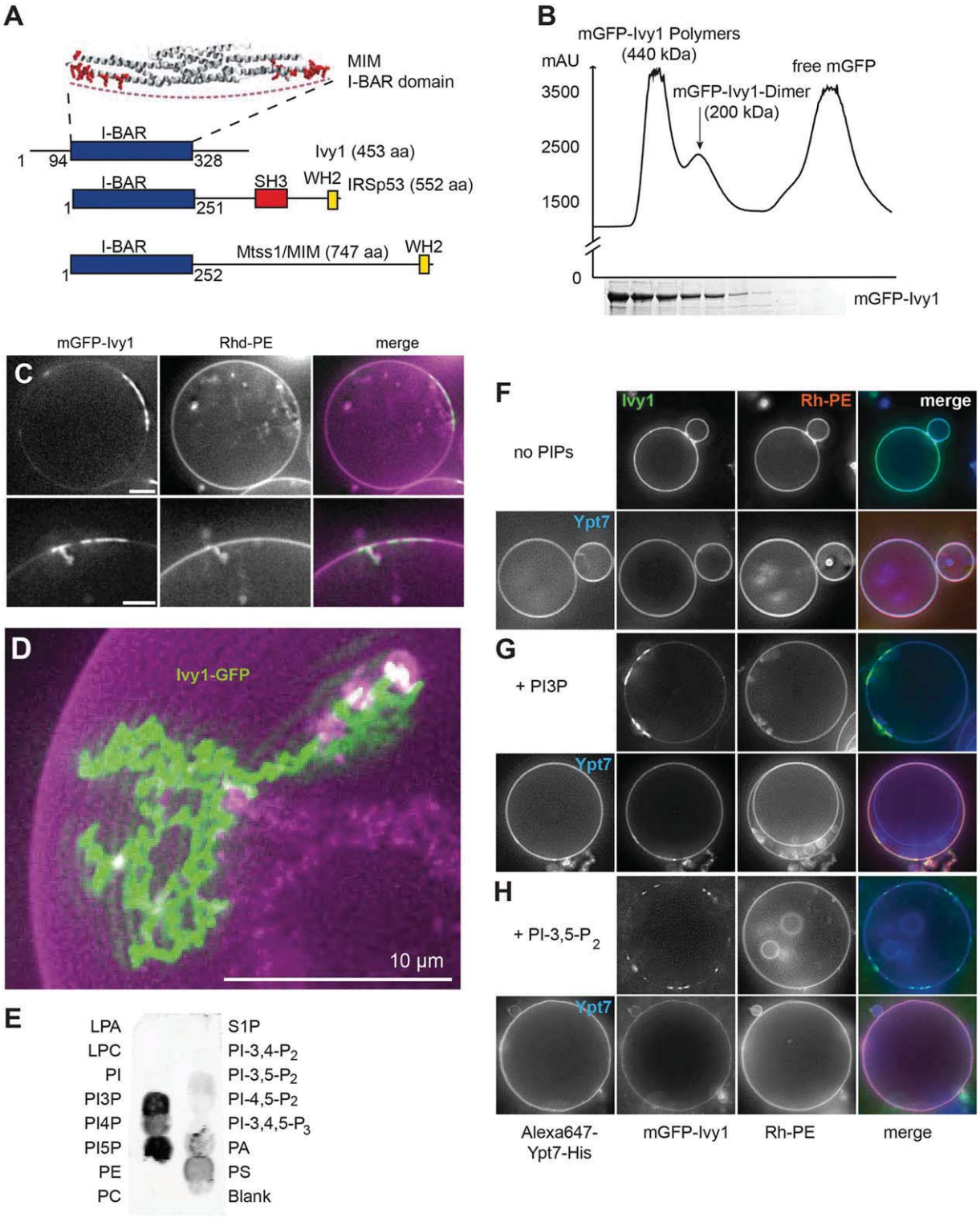

Fig. 6. See next page for legend.

maintaining the vacuolar membrane homeostasis and, thus, affects TORC1 activity.

Self-organization of Ivy1 is influenced by Ypt7 and phosphoinositides

To understand the role of Ivy1 in membrane dynamics, we searched for putative homologues by using HHpred Software (toolkit.tuebingen.mpg.de/hhpred), and readily identified the mammalian proteins IRSp53 and missing-in-metastasis (MIM) (Mattila et al., 2007). These proteins share with Ivy1 a central I-BAR/IMD domain, but the homology does not extend to regions outside this motif (Fig. 6A). IRSp53 and MIM are both involved in the formation of filopodia of mammalian cells, and are able to induce inward protrusions on liposomes (Becalska et al., 2013; Mattila et al., 2007). To analyze the

Fig. 6. Ivy1 localizes to membrane domains in a PI3P dependent manner. (A) Alignment of Ivy1 with other I-BAR proteins based on a HHPred search. Top, model of the I-BAR domain of MIM taken from (Mattila et al., 2007). Bottom, domain organization of Ivy1, IRSp53 and MIM. In addition to the I-BAR domain, the latter two proteins contain SH3 and/or WH2 domains that are involved in protein-protein interactions. (B) Purification of His-mGFP-tagged Ivy1. Ivy1 was purified through a His-tag, eluted with SUMO protease and then applied to a superdex 200 column. Fractions were analyzed for protein content by using UV spectroscopy (top) and purity by SDS-PAGE and Coomassie staining (bottom); mAU, milliabsorbance units. (C) Domain formation by Ivy1. mGFP-Ivy1 was titrated to giant unilamellar vesicle (GUV) membranes that contained rhodamine-phosphatidylethanolamine (Rhd-DHPE) as a lipid dye. Domain formation was observed only at low concentrations of Ivy1. The bottom panel shows an enlarged section of a domain of a corresponding GUV shown in the top panel. Z-stacks of up to 50 focal planes, taken in 500 nm steps, were recorded to monitor domain localization of Ivy1. GUVs had the following lipid composition: 52.6 mol% dioleoyl (DO)-phosphatidylcholine (PC), 18 mol% DO-phophatidylethanolamine (PE), 5 mol% DO-phosphatidylserine (PS), 8 mol% ergosterol, 3 mol% PI3P, PI-4,5-P_2, 10 mol% DOGS-NTA, 0.4 mol% Rhd-DHPE. Scale bar: 10 µm. (D) Close-up view of Ivy1 domains on a GUV. 20 focal planes of a GUV, recorded in 500 nm steps, were merged into a single plane by maximum intensity projection. Composition and analysis was as in C. Scale bar: 10 µm. (E) Phospholipid preference of Ivy1. His-Ivy1 was incubated with a nitrocellulose strip displaying the selected head groups of the indicated phospholipids, then washed and decorated with an antibody against Ivy1. LPA, lysophosphatidic acid; LPC, lysophosphatidylcholine; PI, phosphatidylinositol; PE, phosphatidylethanolamine; PC, phosphatidylcholine; S1P, sphingosine-1-phosphate; PA, phosphatidic acid; PS, phosphatidylserine. For phosphatidyl-inositol-phosphates such as PI3P, phosphatidyl-inositol-3-phosphate, the phosphorylated residues of the head group are indicated. (F-G) Effect of phosphoinositides and Ypt7 on Ivy1-mediated domain formation on GUVs. Ypt7 with a C-terminal hexahistidine tag was labeled by addition of the maleimide derivative of Alexa-Fluor-647 and targeted onto the membranes through DOGS-NTA lipids, purified by a small gel-filtration column and added to GUVs prior to Ivy1 addition. Domain localization of mGFP-Ivy1 was monitored as before. Where indicated, Ypt7 was present in the GUV preparation. Lipid composition was as follows: 55.6 mol% DOPC, 18 mol% DOPE, DOPS 5 mol%, 8 mol% ergosterol, 3 mol% PI3P, or PI-3,5-P_2, PI-4,5-P_2, 10 mol% DOGS-NTA, 0.4 mol% Rhd-DHPE.

function of Ivy1 on membranes, we purified full-length Ivy1 with a N-terminal mGFP tag that – unlike the isolated I-BAR domain – worked well during the biochemical characterization (our unpublished observations). Gel filtration of the purified protein resulted in a substantial high-molecular-mass peak indicative of multimerization, and a clearly distinct fraction of dimeric protein. As BAR domain proteins form dimers in solution (Frost et al., 2009; Mattila et al., 2007), we used this fraction for further experiments (Fig. 6B).

To analyze Ivy1, we prepared giant unilamellar vesicles (GUVs) by using a vacuolar lipid composition that supports efficient fusion of liposomes that carry vacuolar SNAREs (Mima and Wickner, 2009; Mima et al., 2008; Stroupe et al., 2009; Zinser et al., 1991). We then added Ivy1 to those GUVs. Strikingly, Ivy1 localized to specific domains that often contained invaginated or deformed membranes (Fig. 6C). Localization of Ivy1 to the GUV surface did not require Ypt7, presumably because its ability to recognize the membrane surface itself, even though Ypt7 has a profound effect on Ivy1 behavior (see below). Occasionally, Ivy1 was also found within such invaginations, which agrees with an active role of Ivy1 in inward membrane remodeling (Fig. 6C, bottom). As these domains were rather stable, we were, however, unable to determine whether Ivy1 senses or induces membrane perturbation. A close-up view indicated that Ivy1 polymerized into scaffold-like structures along the GUV membrane, in agreement with its ability to self-interact (Fig. 3E), form domains *in vivo* (Fig. 2A) and self-associate into multimer *in vitro* (Fig. 6B).

As Ivy1 binds directly to Ypt7-GTP (Fig. 2C) and interacts with phosphoinositides, such as phosphatidylinositol (3)-phosphate (PI3P) (Fig. 6E), we tested the influence of either factor on the behavior of Ivy1 on GUVs. When we incubated Ivy1 with GUVs that lacked phosphoinositides, Ivy1 was homogenously distributed over the entire membrane (Fig. 6F). Again, domain localization of Ivy1 was observed in the presence of PI3P but also in that of phosphatidylinositol (3,5)-bisphosphate (PI-3,5-P_2), which are both present on the yeast vacuoles (Fig. 6G,H, top rows). We then tagged Ypt7 at its C terminus with hexahistidine and added this fusion protein to GUVs containing DOGS-NTA lipids (1,2-dioleoyl-*sn*-glycero-3-[(N-(5-amino-1-carboxypentyl)iminodiacetic acid)succinyl]), and Ypt7 was correctly recruited to the GUV membrane. Interestingly, the addition of Ypt7-GTP prevented the domain formation of Ivy1 on membranes (Fig. 6G,H, bottom rows). This suggests that the amount of Ypt7-GTP and of PI3P on vacuole membranes affects the degree of Ivy1-dependent domain formation and, thus, function *in vivo*.

Ivy1 localizes to invaginations at the vacuolar surface

Owing to its behavior *in vitro*, we postulated that Ivy1 has a similar role *in vivo*. We, thus, analyzed the effect of the mutation of eight positively charged residues within the I-BAR domain had on Ivy1 function; the residues were identified on the basis of homology modeling, by using the IRSp53 structure (Lee et al., 2007) as a template. This mutated version of Ivy1 was unable to complement the defects in an *ivy1*Δ *vma16*Δ mutant regarding vacuolar morphology and rapamycin hypersensitivity (Fig. 7A,B), suggesting that these residues within the predicted I-BAR domain are important for Ivy1 function.

Furthermore, we hypothesized that Ivy1 acts during microautophagy that had previously been observed in response to nitrogen starvation (Muller et al., 2000) or in situations of stress, such as starvation (Toulmay and Prinz, 2012; Wang et al., 2014). During starvation, we – indeed – found Ivy1-GFP in microautophagic invaginations in 18% of the vacuoles (Fig. 7C). Recent work indicated that the vacuole membrane forms distinct domains upon prolonged starvation, and Ivy1 was identified as one of the marker proteins for such domains (Toulmay and Prinz, 2013; Wang et al., 2014). The localization to these domains is strongly affected by the alteration of PI3P levels (Fig. 7D). If Ivy1 were to accumulate on such domains and induce a negative curvature, it might be able to regulate membrane content, stabilize negative curvature, or support membrane protein degradation. We reasoned that prolonged heat would induce sufficient stress to vacuoles in order to distinguish between these options and, thus, followed the fate of Ivy1-GFP before and after prolonged heat shock (Fig. 7E-G). We, indeed, observed a dramatic relocalization of Ivy1-GFP from a dot-like location on the vacuole membrane to domains with high negative curvature (Fig. 7E), which is in agreement with the predicted membrane preference of the I-BAR domain within Ivy1. Ivy1 was almost exclusively in domains of negative curvature (Fig. 7F, enlarged area, 7G), which became stable over time and are probably not microautophagy intermediates but, rather, are required to stabilize the vacuole during heat shock. Their appearance was similar to the sterol-rich domains recently described for vacuoles of cells in stationary phase (Toulmay and Prinz, 2013; Wang et al., 2014). However, Ivy1 is not necessary for the induction or maintenance of these membrane invaginations and domain formation (marked here with Ego1-GFP), because the *ivy1*Δ mutant shows the same vacuolar morphology under conditions of heat shock (Fig. 7H). Importantly, this assay shows that Ivy1 has, indeed, a preference for negative curvature as predicted from its domain structure.

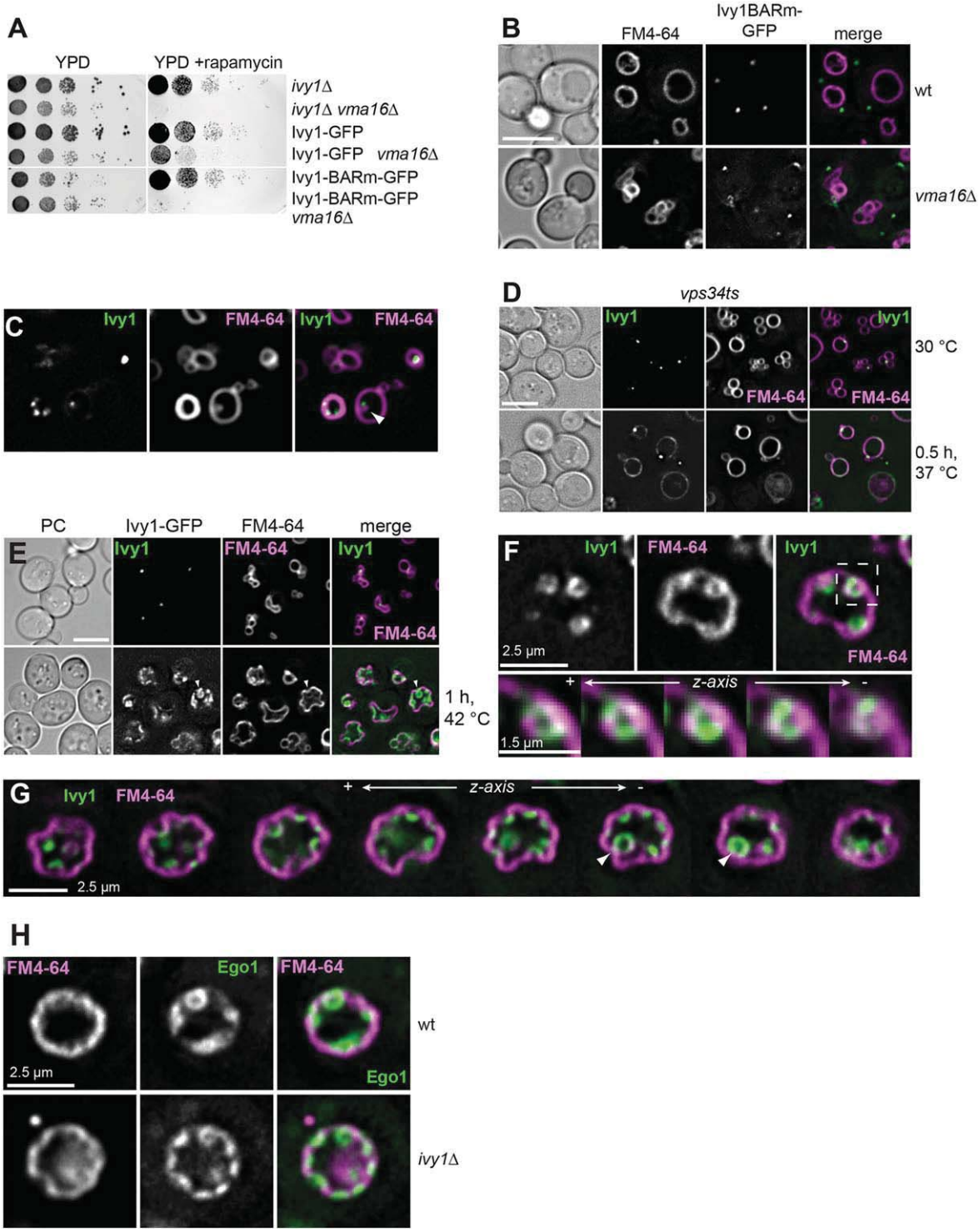

Fig. 7. Ivy1 marks sites of negative curvature on vacuoles involved in the maintenance of membrane homeostasis. (A,B) Analysis of I-BAR mutations in Ivy1. Ivy1 was modeled onto the I-BAR structure of IRSp53, a close homolog of MIM (pdb code: 2YKT) via swissmodel (www.swissmodel.expasy.org). Eight positively charged residues along the postulated membrane interaction site (K102, 106, 203, 209, 216, 227, R220, 231) were mutated to alanine and mutants were analyzed as GFP-tagged proteins for growth on rapamycin (A) and localization in *ivy1*Δ (B, top) and *ivy1*Δ *vma16*Δ cells (B, bottom). Scale bar: 5 µm. (C) Ivy1-GFP localizes to vacuolar invaginations upon nitrogen starvation. Cells expressing Ivy1-GFP were grown to logarithmic growth phase, stained with FM4-64, starved for nitrogen for 1 h and subsequently analyzed by fluorescence microscopy. In 18% of counted vacuoles (*n*=200) Ivy1-GFP was observed on microautophagic invaginations. (D) Ivy1 localization to dots depends on PI3P availability. A temperature sensitive vps34 strain expressing Ivy1-GFP was grown at 26°C or at 37°C for one hour and then analyzed by fluorescence microscopy. Scale bar: 5 µm. (E–G) Ivy1-GFP localizes to invaginations at the vacuole upon heat stress. Cells expressing Ivy1-GFP were grown to logarithmic growth phase, stained with FM4-64 and analyzed by fluorescence microscopy before and after 1 h heat shock at 42°C. Overviews are seen in E. The enlarged picture of a single vacuole shown in F highlights vesicular structure at the vacuole surface positive for Ivy1. Eight focal planes of a Z-stack of a single vacuole are shown in G. Scale bar in E, 5 µm; in F,G 2.5 µm; in consecutive stacks of F, 1.5 µm. (H) Invaginations form in the absence of Ivy1. Ego1-GFP was followed relative to FM4-64-stained vacuoles by fluorescence microscopy in wild-type (wt) and *ivy1*Δ cells. Scale bar: 2.5 µm.

Our *in vitro* experiments showed that Ivy1 interacts with several phosphoinositides (Fig. 6E), and that the presence of PI3P or PI-3,5-P_2 might affect the behavior of Ivy1 on membranes (Fig. 6F–H). We, thus, analyzed mutants affecting PIP levels on vacuoles and noticed that the deletion of Fab1 – the PI-3,5-kinase of yeast – which results in a very large vacuole (Gary et al., 1998), led to a redistribution of Ivy1-GFP from a dot-like to a more homogenous localization along the vacuole surface (see below). The same large vacuole phenotype has been observed in several other mutants involved in PI-3,5-P2 biogenesis, such as *atg18*Δ, *vac7*Δ and *fig4*Δ, suggesting that membrane turnover is be defective (Duex et al., 2006; Gary et al., 2002). We, thus, asked whether Ivy1 is a marker that can be used to observe membrane remodeling upon Fab1 induction. For this, we placed *FAB1* under control of the inducible *GAL1* promotor, which represses Fab1 production in the presence of glucose and mimics the deletion phenotype (Fig. 8A) (Gary et al., 1998). Like in the deletion phenotype, Ivy1-GFP was distributed over the entire vacuole surface (Fig. 8A). When we induced Fab1 by adding galactose, we frequently observed Ivy1 in dots within the vacuole lumen (Fig. 8A,B). As these structures did not stain well with FM4-64, we are not yet sure whether Ivy1 just localizes to or induces these structures. However, the location of Ivy1, again, implies a role in microautophagy events. Ivy1 seems to be induced during starvation, which also results in accumulation of lipid droplets proximal to the vacuole (Wang et al., 2014). Therefore, we asked whether Ivy1 localization correlates with alterations of the vacuolar surface. We grew cells for several days and observed Ivy1 localization (Fig. 8C). Whereas Ivy1 remained in dots until the diauxic shift, it accumulated in domains on the vacuole during stationary phase. Some Ivy1 protein became visible within the vacuole lumen after 4 days, suggesting that a small fraction of Ivy1 is degraded during microautophagy, which is known to occur in cells in stationary phase. However, the main fraction of Ivy1 protein remained stable within the cell, and we did not observe massive degradation of Ivy1 under these circumstances. Together, our data provide evidence that the I-BAR protein Ivy1 is involved in vacuole membrane homeostasis. Moreover, it is probably the first protein that can be specifically used as a marker protein in order to visualize microautophagy processes at the vacuole.

DISCUSSION

Our data demonstrate that Ivy1 is a novel Ypt7 effector, which controls membrane homeostasis of the yeast vacuole. Ivy1 requires Ypt7 for its recruitment to vacuoles, and its function is controlled by the PI3P content on the surface of this organelle. Ivy1 strongly colocalizes and interacts with the EGO complex, suggesting that it is involved in regulating TORC1 activity. Its main function seems to be the regulation of membrane homeostasis of the vacuole, probably together with other proteins. In agreement with this notion, we observed that the concomitant loss of Ivy1 and the V-ATPase subunits results in a strong expansion of the vacuolar surface with multiple invaginations, which indicates that Ivy1 is a factor required to reduce vacuolar membrane. Taking GUV membranes as a model system, we further show that Ivy1 can self-organize into distinct membrane microcompartments that require PI3P and are modulated by the Ypt7 content (Fig. 6). This analysis also revealed that Ivy1 has a preference for negative curvature. To understand its organization *in vivo*, we searched for conditions, where vacuoles would require such proteins and identified Ivy1 in vacuolar domains of negative curvature that formed during microautophagy, starvation and response to heat shock. The close connection to Ypt7 and the EGO complex suggest that Ivy1 connects trafficking and signaling processes in the context of vacuole membrane biogenesis.

Ivy1 was initially thought to be implicated in endocytic trafficking because its overproduction resulted in vacuole fragmentation and the appearance of MVBs (Lazar et al., 2002). However, we consider this unlikely because – even though we also observed a similar impact on vacuole biogenesis and endocytic trafficking (Fig. 1) – this defect required massive overexpression of Ivy1, which leads to an accumulation of Ivy1 deposits proximal to MVBs and vacuoles (Fig. 1C-F). Similarly, the inhibition of the vacuole fusion assay is the simple consequence of the ability of Ivy1 to bind Ypt7-GTP on vacuoles. In the same study, the HOPS subunit Vps33 was suggested to be a main binding partner of Ivy1 (Lazar et al., 2002) but, so far, we did not find evidence for this. Ivy1 overexpression did not affect relocalization of Vps33 to vacuolar membranes (whereas Ypt7 was clustered on vacuoles) and Vps33 deletion did not affect Ivy1 localization (Fig. 2). The previously observed rescue of Ivy1-induced vacuole fragmentation in response to Vps33 overexpression could be a consequence of better stability of the HOPS complex on vacuoles. Whether Vps33 is involved in the localization of HOPS with the EGO complex and Ivy1 on vacuolar membranes will require further analyses.

Our data provide strong arguments in favour of a so-far-unknown Ypt7-dependent function of Ivy1 in the organization of the vacuolar membrane (Fig. 8D). Athough Ivy1 is not required for the formation of vacuolar domains (Toulmay and Prinz, 2013) or the localization of the EGO complex (shown here), it strongly accumulates in distinct membrane subdomanins on the vacuole together with the EGO complex, Ypt7 and Vps39 as one of the tested HOPS subunits (Fig. 2) (Binda et al., 2009). These domains are proximal to the previously characterized contact site for vacuoles and mitochondria or endosomes, suggesting that this zone provides a template for the assembly of multiple membrane proteins. Strikingly, Ivy1 participates to a distinct sterol-rich domain on vacuoles that is enriched under conditions of starvation (Toulmay and Prinz, 2013). Recent data further show that the same vacuolar domains are the site of starvation-induced lipophagy (Wang et al., 2014), which is a long-term adaptation of cells to nutrient deprivation. This process depends on a number of autophagy proteins, including the autophagy-specific PI3-kinase complex (van Zutphen et al., 2014; Wang et al., 2014). Ivy1 strongly localizes to these zones together with the PI3-kinase complex during stationary phase (Wang et al., 2014). We believe that the massively enlarged vacuolar membrane in mutants lacking Ivy1 and V-ATPase subunits could be the result of a defect in the organization of this subdomain that, consequently, affects microautophagy and signaling through the EGO complex. Potentially, Ypt7 binding by Ivy1 also limits the available Ypt7 pool and, thus, favors lipophagy and other types of microautophagy under conditions of starvation, thus providing a convenient shift from trafficking to (micro)autophagy programs.

Recently, a new I-BAR protein that affects phagocytosis and cytokinesis was characterized in *Dictyostelium discoideum* (Linkner et al., 2014). Like Ivy1, IBARa localizes to the vacuole in a PI3P-dependent manner and does not seem to affect the formation of filopodia. However, unlike Ivy1, IBARa is basically reduced to its I-BAR domain, which – by itself – induces liposome invaginations. Even though the cellular phenotypes upon IBARa deletion suggest a direct role in phagocytosis, the precise function of the protein *in vivo* remains elusive. Our data also did not reveal whether Ivy1 itself drives protrusions into the vacuole, although we located the protein exactly at these sites. Furthermore, the function of Ivy1 might be regulated post-translationally. Because the isolated I-BAR domain of Ivy1 was insoluble following overexpression, we were unable to test its ability to deform membranes. However,

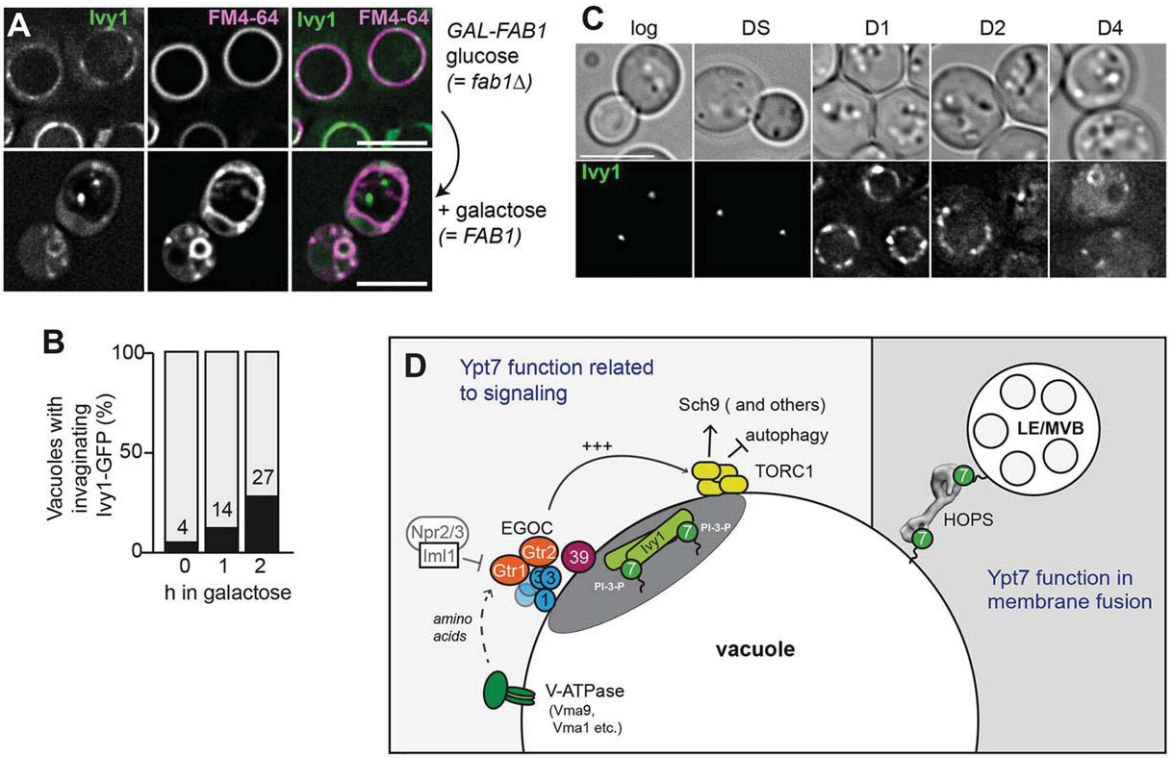

Fig. 8. Ivy1 is present at site of microautophagy. (A,B) Ivy1-GFP localizes to vacuolar invaginations dependent on the Fab1 kinase. Cells expressing *FAB1* from the *GAL1* promotor and Ivy1-GFP were grown in YPD to logarithmic growth phase and stained for FM4-64 (A). To induce expression of *FAB1*, cells were washed twice with sterile water and incubated for 1 or 2 h in YPG. Cells were analyzed for localization of Ivy1-GFP by fluorescence microscopy. Scale bars: 5 µm. Panel B shows a quantification of the localization of Ivy1-GFP to vacuolar invaginations for each time point. (C) Localization of Ivy1 during starvation. Yeast cells were grown from logarithmic phase (log) to saturation, which result in diauxic shift (DS). Samples were collected at day one (D1), two (D2) and four (D4) and analyzed immediately by fluorescence microscopy for Ivy1-GFP localization as before. (D) Model of Ypt7-dependent functions related to signaling and fusion. To the left, Ypt7-dependent localization of Ivy1 to a vacuolar domain is shown relative to the Ego complex (EGOC) and its regulator, the Iml1 complex. Activation of TORC1 and the cellular consequences are shown. To the right, Ypt7 interaction with the HOPS complex during tethering of late endosomes (LE)/multivesicular bodies (MVB) is illustrated. 1, Ego1; 3, Ego3; 7, Ypt7; 39, Vps39.

neither Ivy1 overexpression nor the addition of full-length Ivy1 to GUVs (Fig. 6) seemed to result in the induction of protrusions. We, thus, consider it more likely that Ivy1 follows and, possibly, promotes negative membrane curvature, rather than inducing it. Future analyses of Ivy1 mutants will be necessary to dissect this issue in more detail.

In summary, our data provide a molecular link of an I-BAR protein to the Rab7-like Ypt7 GTPase and, possibly, to the PI3P content on vacuoles. Moreover, they suggests a crosstalk between one of the main nutrient-sensing signal cascades and microautophagy (Fig. 8D), resulting in an attractive model outlining the regulation of vacuolar membrane homeostasis as an adaptation to nutrient availability.

MATERIALS AND METHODS

Yeast strains and plasmids

All yeast strains used in this study are listed in supplementary material Table S1. For cloning, *IVY1* coding sequence was amplified from *S. cerevisiae* genomic DNA with Phusion polymerase (Thermo Scientific) and cloned into *E. coli* expression vectors. Plasmids were transformed into *E. coli* BL21 (DE3) Rosetta cells.

To overproduce Ivy1 from *E. coli* with an N-terminal His-tag, the coding region of *IVY1* was cloned into the *Bam*HI/*Xho*I sites of a pET32c vector. To generate mGFP-tagged Ivy1, *IVY1* was cloned into the *Bam*HI/*Xho*I sites of a pCOLAHS vector. Afterwards, mGFP was cloned in front of *IVY1* into the *Bam*HI/*Bgl*II sites of the pCOLAHS vector, that had been digested with *Bam*HI. The pCOLAHS vector was derived from the pCOLADuet1 vector by cloning a SUMO-tag in frame with the His-tag. All plasmids are listed in supplementary material Table S2.

Vacuole fusion assay

The fusion assay employs two sets of isolated vacuoles. One lacks the alkaline phosphatase Pho8 but contains a full set of proteases, whereas the other contains the alkaline phosphatase as the inactive pro-form owing to the absence of the Pep4-protease. During fusion, lumenal mixing results in cleavage and activation of Pho8, which can be assayed spectrophotometrically (Cabrera and Ungermann, 2008). Vacuoles were purified from strains BJ3505 (*pep4*Δ) and DKY6281 (*pho8*Δ). Fusion reactions containing 3 µg of each vacuole type were performed in fusion reaction buffer (10 mM PIPES/KOH pH 6.8, 5 mM $MgCl_2$, 125 mM KCl, 0.2 M sorbitol), containing an ATP-regenerating system. Reactions were incubated for 90 min at 26°C, and then developed as described (LaGrassa and Ungermann, 2005).

Fluorescence microscopy

For microscopy, yeast cells were grown in yeast peptone dextrose (YPD) medium, yeast peptone galactose (YPG) or in selective medium to an OD_{600} of about 1, collected by centrifugation (3 min at 4000 ***g***, 20°C), washed with synthetic medium containing either glucose or galactose, and immediately analyzed by using fluorescence microscopy. Staining of the cells with FM4-64 was performed as described (LaGrassa and Ungermann, 2005). In brief, cells were incubated with 30 µM FM4-64 for 30 min, washed with the corresponding medium and further incubated for 1.5 h in fresh medium. Images were acquired using a Leica DM5500 B microscope equipped with a SPOT Pursuit camera with GFP, RFP, FM4-64 and DIC (differential interference contrast) filters or using a DeltaVision Elite fluorescence microscope (Applied Precision, Issaquah, WA) equipped with a CoolSNAP HQ Camera using FITC, YFP, TRITC, DAPI and mCherry filters. Images acquired with the Leica microscope were deconvolved using the Metamorph software. Images acquired with DeltaVision Elite were

deconvolved using SoftWorx. Pictures were processed using Adobe Photoshop CS4 or ImageJ.

Bimolecular fluorescence complementation assay

The tagging of genes of interest for the bimolecular fluorescence complementation assay (BiFC, also known as split-YFP approach) was carried out as described (Sung and Huh, 2007). In brief, proteins of interest are tagged either with the N-terminus or the C-terminus of the Venus fluorescent protein. Complementation of Venus fluorescence was examined by using the YFP fluorescence channel.

Electron microscopy analyses

Examination of yeast cells by electron microscopy and IEM was carried out as described (Griffith et al., 2008). For the IEM, cells were fixed, embedded in gelatin and cryo-sectioned. This was followed by immuno-labeling with an anti-GFP antibody (Abcam) and by protein-A–gold incubation to localize Ivy1. Sections were analysed by using an electron microscope (1200 EX; JEOL).

Measurement of TORC1 activity through phosphorylation of Sch9

TORC1 activity was measured as described (Urban et al., 2007). Phosphorylation of the C-terminal part of HA-tagged Sch9 was used as readout for TORC1 activity. In brief, whole-protein extracts were prepared, treated with 2-nitro-5-thiocyanatobenzoic acid (NTCB), and further analyzed by SDS-PAGE and western blotting. Sch9 was visualized by decoration with anti-HA. Quantification of TORC1 activity was carried out as previously reported (Binda et al., 2009). Wild-type TORC1 activity was set to 100%.

Rab GTPase pulldown

The glutathione–Rab pull-down experiment was done as described before (Markgraf et al., 2009). recombinant GST-tagged Rab proteins were loaded with 1 mM GDP or GTPS in 20 mM HEPES/NaOH pH 7.4. 150 µg Rab proteins were coupled to GSH beads. Rab proteins were incubated with recombinant His-tagged Ivy1 (or control proteins) for 1 h at 4°C on a nutator mixer. Beads were washed three times with 20 mM HEPES-NaOH, 100 mM NaCl, 1 mM MgCl, 0.1% (w/v) Triton X-100, and proteins were eluted with 20 mM HEPES-NaOH, 100 mM NaCl, 1 mM MgCl, 0.1% (w/v) TritonX-100+20 mM EDTA. The eluates were then precipitated with trichloracetic acid (TCA), and analyzed by SDS-PAGE and western blotting. As a loading control, the bound GST–Rab GTPase was eluted from the beads by boiling in sample buffer, and analyzed by SDS-PAGE and Coomassie staining.

Purification of recombinant Ivy1

E. coli BL21 (DE3) Rosetta cells containing the *IVY1*-plasmids or *YPT7*/*VPS21*-plasmids were grown until OD_{600} of 0.8; expression was induced with 0.5 mM IPTG overnight at 16°C. Cells were harvested and lysed in 50 mM Tris/HCl pH 7.5, 150 mM NaCl, 1 mM PMSF, 1× protease inhibitor cocktail; 1×=0.1 mg/ml of leupeptin, 1 mM o-phenanthroline, 0.5 mg/ml of pepstatin A, 0.1 mM Pefabloc. Lysates were centrifuged 15 min at 30,000 ***g*** and the cleared supernatant was added to Ni-NTA beads for His-tagged protein or to GSH-beads for GST-tagged protein, followed by an incubation for 1 h at 4°C on a nutator mixer. Ni-NTA-beads were washed with 25 ml buffer containing 20 mM imidazole. His-tagged Ivy1 was eluted from beads with buffer containing 0.3 M imidazole. His-SUMO-mGFP-Ivy1 was eluted using the SUMO protease. GST-Ivy1 was eluted using buffer containing 15 mM reduced glutathione. The buffer was finally exchanged by dialyzing the eluted proteins against 10 mM PIPES/KOH pH 6.8, 200 mM sorbitol, 150 mM KCl, 5 mM $MgCl_2$ containing 10% glycerol.

Preparation of giant unilamellar vesicles (GUVs)

Giant unilamellar vesicles (GUVs) were prepared by electroformation as described before (Romanov et al., 2012). Different lipid compositions were used as indicated in the figure legends. Lipids were from Avanti polar lipids and Echelon Biosciences.

Tandem affinity purification

Tandem affinity purification (TAP) of HOPS complex was carried out as described (Ostrowicz et al., 2010; Puig et al., 2001). In brief, logarithmically growing yeast cells were lysed in 50 mM HEPES/NaOH pH 7.4, 150 mM NaCl, 1.5 mM $MgCl_2$, centrifuged for 10 min at 20,000 ***g*** and 1 h at 100,000 ***g***. The cleared lysate was incubated for 1 h with IgG Sepharose beads. Bound protein was eluted using TEV protease. Eluates were analyzed using SDS-PAGE and western blotting.

Acknowledgements

We thank Markus Babst for suggestions and members of the Ungermann lab for discussions. This work was supported by the DFG (UN111/7-1), the SFB 944 (project P11) and by the Hans-Mühlenhoff foundation (to C.U.), and the Swiss National Foundation (to C.D.V.). F.R. is supported by ECHO (700.59.003), ALW Open Program (821.02.017 and 822.02.014), DFG-NWO cooperation (DN82-303) and ZonMW VICI (016.130.606) grants.

Competing interests

The authors declare no competing or financial interests.

Author contributions

J.N., M.P.G., H.A., A.S. and J.G. performed experiments and analyzed data; T.L. and S.E.V. performed bioinformatic analyses; J.N., F.R., C.D.V. and C.U. devised the study, analyzed experiments and wrote the manuscript.

Funding

This research received no specific grant from any funding agency in the public, commercial or not-for-profit sectors.

Supplementary material

Supplementary material available online

References

Arlt, H., Perz, A. and Ungermann, C. (2011). An overexpression screen in Saccharomyces cerevisiae identifies novel genes that affect endocytic protein trafficking. *Traffic* **12**, 1592-1603.

Balderhaar, H. J. K., Arlt, H., Ostrowicz, C., Bröcker, C., Sündermann, F., Brandt, R., Babst, M. and Ungermann, C. (2010). The Rab GTPase Ypt7 is linked to retromer-mediated receptor recycling and fusion at the yeast late endosome. *J. Cell Sci.* **123**, 4085-4094.

Bar-Peled, L. and Sabatini, D. M. (2012). SnapShot: mTORC1 signaling at the lysosomal surface. *Cell* **151**, 1390-1390.e1.

Bar-Peled, L., Schweitzer, L. D., Zoncu, R. and Sabatini, D. M. (2012). Ragulator is a GEF for the Rag GTPases that signal amino acid levels to mTORC1. *Cell* **150**, 1196-1208.

Bar-Peled, L., Chantranupong, L., Cherniack, A. D., Chen, W. W., Ottina, K. A., Grabiner, B. C., Spear, E. D., Carter, S. L., Meyerson, M. and Sabatini, D. M. (2013). A tumor suppressor complex with GAP activity for the Rag GTPases that signal amino acid sufficiency to mTORC1. *Science* **340**, 1100-1106.

Becalska, A. N., Kelley, C. F., Berciu, C., Stanishneva-Konovalova, T. B., Fu, X., Wang, S., Sokolova, O. S., Nicastro, D. and Rodal, A. A. (2013). Formation of membrane ridges and scallops by the F-BAR protein Nervous Wreck. *Mol. Biol. Cell* **24**, 2406-2418.

Berchtold, D. and Walther, T. C. (2009). TORC2 plasma membrane localization is essential for cell viability and restricted to a distinct domain. *Mol. Biol. Cell* **20**, 1565-1575.

Bernales, S., McDonald, K. L. and Walter, P. (2006). Autophagy counterbalances endoplasmic reticulum expansion during the unfolded protein response. *PLoS Biol.* **4**, e423.

Binda, M., Péli-Gulli, M.-P., Bonfils, G., Panchaud, N., Urban, J., Sturgill, T. W., Loewith, R. and de Virgilio, C. (2009). The Vam6 GEF controls TORC1 by activating the EGO complex. *Mol. Cell* **35**, 563-573.

Böckler, S. and Westermann, B. (2014). Mitochondrial ER contacts are crucial for mitophagy in yeast. *Dev. Cell* **28**, 450-458.

Bonfils, G., Jaquenoud, M., Bontron, S., Ostrowicz, C., Ungermann, C. and de Virgilio, C. (2012). Leucyl-tRNA synthetase controls TORC1 via the EGO complex. *Mol. Cell* **46**, 105-110.

Brett, C. L. and Merz, A. J. (2008). Osmotic regulation of Rab-mediated organelle docking. *Curr. Biol.* **18**, 1072-1077.

Bröcker, C., Kuhlee, A., Gatsogiannis, C., Kleine Balderhaar, H. J., Hönscher, C., Engelbrecht-Vandré, S., Ungermann, C. and Raunser, S. (2012). Molecular architecture of the multisubunit homotypic fusion and vacuole protein sorting (HOPS) tethering complex. *Proc. Natl. Acad. Sci. USA* **109**, 1991-1996.

Cabrera, M. and Ungermann, C. (2008). Purification and in vitro analysis of yeast vacuoles. *Methods Enzymol.* **451**, 177-196.

Cabrera, M., Ostrowicz, C. W., Mari, M., LaGrassa, T. J., Reggiori, F. and Ungermann, C. (2009). Vps41 phosphorylation and the Rab Ypt7 control the

targeting of the HOPS complex to endosome-vacuole fusion sites. *Mol. Biol. Cell* **20**, 1937-1948.
Chen, Y. and Klionsky, D. J. (2011). The regulation of autophagy - unanswered questions. *J. Cell Sci.* **124**, 161-170.
Cui, Y., Zhao, Q., Gao, C., Ding, Y., Zeng, Y., Ueda, T., Nakano, A. and Jiang, L. (2014). Activation of the Rab7 GTPase by the MON1-CCZ1 Complex Is Essential for PVC-to-Vacuole Trafficking and Plant Growth in Arabidopsis. *Plant Cell* **26**, 2080-2097.
Dubouloz, F., Deloche, O., Wanke, V., Cameroni, E. and de Virgilio, C. (2005). The TOR and EGO protein complexes orchestrate microautophagy in yeast. *Mol. Cell* **19**, 15-26.
Duex, J. E., Tang, F. and Weisman, L. S. (2006). The Vac14p-Fig4p complex acts independently of Vac7p and couples PI3,5P2 synthesis and turnover. *J. Cell Biol.* **172**, 693-704.
Durán, R. V. and Hall, M. N. (2012). Regulation of TOR by small GTPases. *EMBO Rep.* **13**, 121-128.
Elbaz-Alon, Y., Rosenfeld-Gur, E., Shinder, V., Futerman, A. H., Geiger, T. and Schuldiner, M. (2014). A dynamic interface between vacuoles and mitochondria in yeast. *Dev. Cell* **30**, 95-102.
Flinn, R. J., Yan, Y., Goswami, S., Parker, P. J. and Backer, J. M. (2010). The late endosome is essential for mTORC1 signaling. *Mol. Biol. Cell* **21**, 833-841.
Frost, A., Unger, V. M. and de Camilli, P. (2009). The BAR domain superfamily: membrane-molding macromolecules. *Cell* **137**, 191-196.
Gary, J. D., Wurmser, A. E., Bonangelino, C. J., Weisman, L. S. and Emr, S. D. (1998). Fab1p is essential for PtdIns(3)P 5-kinase activity and the maintenance of vacuolar size and membrane homeostasis. *J. Cell Biol.* **143**, 65-79.
Gary, J. D., Sato, T. K., Stefan, C. J., Bonangelino, C. J., Weisman, L. S. and Emr, S. D. (2002). Regulation of Fab1 phosphatidylinositol 3-phosphate 5-kinase pathway by Vac7 protein and Fig4, a polyphosphoinositide phosphatase family member. *Mol. Biol. Cell* **13**, 1238-1251.
Gerondopoulos, A., Langemeyer, L., Liang, J.-R., Linford, A. and Barr, F. A. (2012). BLOC-3 mutated in Hermansky-Pudlak syndrome is a Rab32/38 guanine nucleotide exchange factor. *Curr. Biol.* **22**, 2135-2139.
Griffith, J., Mari, M., de Mazière, A. and Reggiori, F. (2008). A cryosectioning procedure for the ultrastructural analysis and the immunogold labelling of yeast Saccharomyces cerevisiae. *Traffic* **9**, 1060-1072.
Haas, A., Conradt, B. and Wickner, W. (1994). G-protein ligands inhibit in vitro reactions of vacuole inheritance. *J. Cell Biol.* **126**, 87-97.
Haas, A., Scheglmann, D., Lazar, T., Gallwitz, D. and Wickner, W. (1995). The GTPase Ypt7p of Saccharomyces cerevisiae is required on both partner vacuoles for the homotypic fusion step of vacuole inheritance. *EMBO J.* **14**, 5258-5270.
Hönscher, C., Mari, M., Auffarth, K., Bohnert, M., Griffith, J., Geerts, W., van der Laan, M., Cabrera, M., Reggiori, F. and Ungermann, C. (2014). Cellular metabolism regulates contact sites between vacuoles and mitochondria. *Dev. Cell* **30**, 86-94.
Hou, H., Subramanian, K., LaGrassa, T. J., Markgraf, D., Dietrich, L. E. P., Urban, J., Decker, N. and Ungermann, C. (2005). The DHHC protein Pfa3 affects vacuole-associated palmitoylation of the fusion factor Vac8. *Proc. Natl. Acad. Sci. USA* **102**, 17366-17371.
Jewell, J. L., Russell, R. C. and Guan, K.-L. (2013). Amino acid signalling upstream of mTOR. *Nat. Rev. Mol. Cell Biol.* **14**, 133-139.
Klionsky, D. J., Abdalla, F. C., Abeliovich, H., Abraham, R. T., Acevedo-Arozena, A., Adeli, K., Agholme, L., Agnello, M., Agostinis, P., Aguirre-Ghiso, J. A. et al. (2012). Guidelines for the use and interpretation of assays for monitoring autophagy. *Autophagy* **8**, 445-544.
LaGrassa, T. J. and Ungermann, C. (2005). The vacuolar kinase Yck3 maintains organelle fragmentation by regulating the HOPS tethering complex. *J. Cell Biol.* **168**, 401-414.
Lazar, T., Scheglmann, D. and Gallwitz, D. (2002). A novel phospholipid-binding protein from the yeast Saccharomyces cerevisiae with dual binding specificities for the transport GTPase Ypt7p and the Sec1-related Vps33p. *Eur. J. Cell Biol.* **81**, 635-646.
Lee, S. H., Kerff, F., Chereau, D., Ferron, F., Klug, A. and Dominguez, R. (2007). Structural basis for the actin-binding function of missing-in-metastasis. *Structure* **15**, 145-155.
Levine, T. P., Daniels, R. D., Wong, L. H., Gatta, A. T., Gerondopoulos, A. and Barr, F. A. (2013). Discovery of new Longin and Roadblock domains that form platforms for small GTPases in Ragulator and TRAPP-II. *Small GTPases* **4**, 62-69.
Linkner, J., Witte, G., Zhao, H., Junemann, A., Nordholz, B., Runge-Wollmann, P., Lappalainen, P. and Faix, J. (2014). The inverse BAR domain protein IBARa drives membrane remodeling to control osmoregulation, phagocytosis and cytokinesis. *J. Cell Sci.* **127**, 1279-1292.
Liu, T.-T., Gomez, T. S., Sackey, B. K., Billadeau, D. D. and Burd, C. G. (2012). Rab GTPase regulation of retromer-mediated cargo export during endosome maturation. *Mol. Biol. Cell* **23**, 2505-2515.
Markgraf, D. F., Ahnert, F., Arlt, H., Mari, M., Peplowska, K., Epp, N., Griffith, J., Reggiori, F. and Ungermann, C. (2009). The CORVET subunit Vps8 cooperates with the Rab5 homolog Vps21 to induce clustering of late endosomal compartments. *Mol. Biol. Cell* **20**, 5276-5289.
Mattila, P. K., Pykäläinen, A., Saarikangas, J., Paavilainen, V. O., Vihinen, H., Jokitalo, E. and Lappalainen, P. (2007). Missing-in-metastasis and IRSp53 deform PI(4,5)P2-rich membranes by an inverse BAR domain-like mechanism. *J. Cell Biol.* **176**, 953-964.
Miaczynska, M., Christoforidis, S., Giner, A., Shevchenko, A., Uttenweiler-Joseph, S., Habermann, B., Wilm, M., Parton, R. G. and Zerial, M. (2004). APPL proteins link Rab5 to nuclear signal transduction via an endosomal compartment. *Cell* **116**, 445-456.
Mima, J. and Wickner, W. (2009). Phosphoinositides and SNARE chaperones synergistically assemble and remodel SNARE complexes for membrane fusion. *Proc. Natl. Acad. Sci. USA* **106**, 16191-16196.
Mima, J., Hickey, C. M., Xu, H., Jun, Y. and Wickner, W. (2008). Reconstituted membrane fusion requires regulatory lipids, SNAREs and synergistic SNARE chaperones. *EMBO J.* **27**, 2031-2042.
Mizushima, N., Yoshimori, T. and Ohsumi, Y. (2011). The role of Atg proteins in autophagosome formation. *Annu. Rev. Cell Dev. Biol.* **27**, 107-132.
Muller, O., Sattler, T., Flotenmeyer, M., Schwarz, H., Plattner, H. and Mayer, A. (2000). Autophagic Tubes. Vacuolar invaginations involved in lateral membrane sorting and inverse vesicle budding. *J. Cell Biol.* **151**, 519-528.
Nickerson, D. P., Russell, M. R. G., Lo, S.-Y., Chapin, H. C., Milnes, J. M. and Merz, A. J. (2012). Termination of isoform-selective Vps21/Rab5 signaling at endolysosomal organelles by Msb3/Gyp3. *Traffic* **13**, 1411-1428.
Nikko, E. and Andre, B. (2007). Split-ubiquitin two-hybrid assay to analyze protein-protein interactions at the endosome: application to Saccharomyces cerevisiae Bro1 interacting with ESCRT complexes, the Doa4 ubiquitin hydrolase, and the Rsp5 ubiquitin ligase. *Eukaryot. Cell* **6**, 1266-1277.
Nordmann, M., Cabrera, M., Perz, A., Bröcker, C., Ostrowicz, C., Engelbrecht-Vandré, S. and Ungermann, C. (2010). The Mon1-Ccz1 complex is the GEF of the late endosomal Rab7 homolog Ypt7. *Curr. Biol.* **20**, 1654-1659.
Numrich, J. and Ungermann, C. (2014). Endocytic Rabs in membrane trafficking and signaling. *Biol. Chem.* **395**, 327-333.
Ostrowicz, C. W., Bröcker, C., Ahnert, F., Nordmann, M., Lachmann, J., Peplowska, K., Perz, A., Auffarth, K., Engelbrecht-Vandré, S. and Ungermann, C. (2010). Defined subunit arrangement and Rab interactions are required for functionality of the HOPS tethering complex. *Traffic* **11**, 1334-1346.
Pan, X., Roberts, P., Chen, Y., Kvam, E., Shulga, N., Huang, K., Lemmon, S. and Goldfarb, D. S. (2000). Nucleus-vacuole junctions in Saccharomyces cerevisiae are formed through the direct interaction of Vac8p with Nvj1p. *Mol. Biol. Cell* **11**, 2445-2457.
Panchaud, N., Peli-Gulli, M.-P. and de Virgilio, C. (2013). Amino acid deprivation inhibits TORC1 through a GTPase-activating protein complex for the Rag family GTPase Gtr1. *Sci. Signal.* **6**, ra42.
Puig, O., Caspary, F., Rigaut, G., Rutz, B., Bouveret, E., Bragado-Nilsson, E., Wilm, M. and Seraphin, B. (2001). The tandem affinity purification (TAP) method: a general procedure of protein complex purification. *Methods* **24**, 218-229.
Roberts, P., Moshitch-Moshkovitz, S., Kvam, E., O'Toole, E., Winey, M. and Goldfarb, D. S. (2003). Piecemeal microautophagy of nucleus in Saccharomyces cerevisiae. *Mol. Biol. Cell* **14**, 129-141.
Romanov, J., Walczak, M., Ibiricu, I., Schüchner, S., Ogris, E., Kraft, C. and Martens, S. (2012). Mechanism and functions of membrane binding by the Atg5-Atg12/Atg16 complex during autophagosome formation. *EMBO J.* **31**, 4304-4317.
Sancak, Y., Bar-Peled, L., Zoncu, R., Markhard, A. L., Nada, S. and Sabatini, D. M. (2010). Ragulator-Rag complex targets mTORC1 to the lysosomal surface and is necessary for its activation by amino acids. *Cell* **141**, 290-303.
Schuck, S., Gallagher, C. M. and Walter, P. (2014). ER-phagy mediates selective degradation of endoplasmic reticulum independently of the core autophagy machinery. *J. Cell Sci.* **127**, 4078-4088.
Seals, D. F., Eitzen, G., Margolis, N., Wickner, W. T. and Price, A. (2000). A Ypt/Rab effector complex containing the Sec1 homolog Vps33p is required for homotypic vacuole fusion. *Proc. Natl. Acad. Sci. USA* **97**, 9402-9407.
Shin, H.-W., Hayashi, M., Christoforidis, S., Lacas-Gervais, S., Hoepfner, S., Wenk, M. R., Modregger, J., Uttenweiler-Joseph, S., Wilm, M., Nystuen, A. et al. (2005). An enzymatic cascade of Rab5 effectors regulates phosphoinositide turnover in the endocytic pathway. *J. Cell Biol.* **170**, 607-618.
Singh, M. L., Krüger, F., Beckmann, H., Brumm, S., Vermeer, J. E. M., Munnik, T., Mayer, U., Stierhof, Y.-D., Grefen, C., Schumacher, K. et al. (2014). Protein delivery to vacuole requires SAND protein-dependent Rab GTPase conversion for MVB-vacuole fusion. *Curr. Biol.* **24**, 1383-1389.
Stein, M.-P., Feng, Y., Cooper, K. L., Welford, A. M. and Wandinger-Ness, A. (2003). Human VPS34 and p150 are Rab7 interacting partners. *Traffic* **4**, 754-771.
Stroupe, C., Hickey, C. M., Mima, J., Burfeind, A. S. and Wickner, W. (2009). Minimal membrane docking requirements revealed by reconstitution of Rab GTPase-dependent membrane fusion from purified components. *Proc. Natl. Acad. Sci. USA* **106**, 17626-17633.
Sturgill, T. W., Cohen, A., Diefenbacher, M., Trautwein, M., Martin, D. E. and Hall, M. N. (2008). TOR1 and TOR2 have distinct locations in live cells. *Eukaryot. Cell* **7**, 1819-1830.

Sung, M.-K. and Huh, W.-K. (2007). Bimolecular fluorescence complementation analysis system for in vivo detection of protein-protein interaction in Saccharomyces cerevisiae. *Yeast* **24**, 767-775.

Thorngren, N., Collins, K. M., Fratti, R. A., Wickner, W. and Merz, A. J. (2004). A soluble SNARE drives rapid docking, bypassing ATP and Sec17/18p for vacuole fusion. *EMBO J.* **23**, 2765-2776.

Tong, A. H. Y., Evangelista, M., Parsons, A. B., Xu, H., Bader, G. D., Page, N., Robinson, M., Raghibizadeh, S., Hogue, C. W. V., Bussey, H. et al. (2001). Systematic genetic analysis with ordered arrays of yeast deletion mutants. *Science* **294**, 2364-2368.

Toulmay, A. and Prinz, W. A. (2012). A conserved membrane-binding domain targets proteins to organelle contact sites. *J. Cell Sci.* **125**, 49-58.

Toulmay, A. and Prinz, W. A. (2013). Direct imaging reveals stable, micrometer-scale lipid domains that segregate proteins in live cells. *J. Cell Biol.* **202**, 35-44.

Urban, J., Soulard, A., Huber, A., Lippman, S., Mukhopadhyay, D., Deloche, O., Wanke, V., Anrather, D., Ammerer, G., Riezman, H. et al. (2007). Sch9 is a major target of TORC1 in Saccharomyces cerevisiae. *Mol. Cell* **26**, 663-674.

van Zutphen, T., Todde, V., de Boer, R., Kreim, M., Hofbauer, H. F., Wolinski, H., Veenhuis, M., van der Klei, I. J. and Kohlwein, S. D. (2014). Lipid droplet autophagy in the yeast Saccharomyces cerevisiae. *Mol. Biol. Cell* **25**, 290-301.

Wang, C.-W., Miao, Y.-H. and Chang, Y.-S. (2014). A sterol-enriched vacuolar microdomain mediates stationary phase lipophagy in budding yeast. *J. Cell Biol.* **206**, 357-366.

Wichmann, H., Hengst, L. and Gallwitz, D. (1992). Endocytosis in yeast: evidence for the involvement of a small GTP-binding protein (Ypt7p). *Cell* **71**, 1131-1142.

Wullschleger, S., Loewith, R. and Hall, M. N. (2006). TOR signaling in growth and metabolism. *Cell* **124**, 471-484.

Wurmser, A. E., Sato, T. K. and Emr, S. D. (2000). New component of the vacuolar class C-Vps complex couples nucleotide exchange on the Ypt7 GTPase to SNARE-dependent docking and fusion. *J. Cell Biol.* **151**, 551-562.

Zhang, T., Péli-Gulli, M.-P., Yang, H., de Virgilio, C. and Ding, J. (2012). Ego3 functions as a homodimer to mediate the interaction between Gtr1-Gtr2 and Ego1 in the EGO complex to activate TORC1. *Structure* **20**, 2151-2160.

Zinser, E., Sperka-Gottlieb, C. D., Fasch, E. V., Kohlwein, S. D., Paltauf, F. and Daum, G. (1991). Phospholipid synthesis and lipid composition of subcellular membranes in the unicellular eukaryote Saccharomyces cerevisiae. *J. Bacteriol.* **173**, 2026-2034.

Zoncu, R., Bar-Peled, L., Efeyan, A., Wang, S., Sancak, Y. and Sabatini, D. M. (2011). mTORC1 senses lysosomal amino acids through an inside-out mechanism that requires the vacuolar H^+-ATPase. *Science* **334**, 678-683.

Zurita-Martinez, S. A., Puria, R., Pan, X., Boeke, J. D. and Cardenas, M. E. (2007). Efficient Tor signaling requires a functional class C Vps protein complex in Saccharomyces cerevisiae. *Genetics* **176**, 2139-2150.